END
DATE
FILMED
4-80
DTIC

AFAPL-TR-79-2107

LEVEL

EXPERIMENTAL INVESTIGATION OF COMPRESSOR ROTOR WAKES

R. P. DRING, H. D. JOSLYN, AND L. W. HARDIN

DTIC
ELECTE
MAR 1 2 1980
C

UNITED TECHNOLOGIES RESEARCH CENTER
EAST HARTFORD, CT 06108

JANUARY 1980

TECHNICAL REPORT AFAPL-TR-79-2107
FINAL REPORT FOR PERIOD 1 SEPTEMBER 1977 - 30 SEPTEMBER 1979

Approved for public release; distribution
unlimited.

AERO PROPULSION LABORATORY
AIR FORCE WRIGHT AERONAUTICAL LABORATORIES
AIR FORCE SYSTEMS COMMAND
WRIGHT-PATTERSON AFB, OHIO 45433

80 3 11 015

ARTHUR J. WENNERSTROM, GS-15
Chief, Compressor Research Group

H. I. BUSH, Deputy Director - GS-15
Turbine Engine Division
Aero Propulsion Laboratory

FOR THE COMMANDER

WALKER H. MITCHELL, GS-15
Chief, Technology Branch

AIR FORCE/56780/21 February 1980 — 200

REPORT DOCUMENTATION PAGE		READ INSTRUCTIONS BEFORE COMPLETING FORM

1. REPORT NUMBER	2. GOVT ACCESSION NO.	3. RECIPIENT'S CATALOG NUMBER
AFAPL-TR-79-2107		

4. TITLE (and Subtitle)

Experimental Investigation of Compressor Rotor Wakes

5. TYPE OF REPORT & PERIOD COVERED

Final Report, Sept. 1977 - Sept. 1979

6. PERFORMING ORG. REPORT NUMBER

UTRC/R79-914183-15

7. AUTHOR(s)

R. P. Dring
H. D. Joslyn
L. W. Hardin

8. CONTRACT OR GRANT NUMBER(s)

F33615-77-C-2083

9. PERFORMING ORGANIZATION NAME AND ADDRESS

United Technologies Research Center
Silver Lane
East Hartford, Conn. 06108

10. PROGRAM ELEMENT, PROJECT, TASK AREA & WORK UNIT NUMBERS

Project 2307
Task S1
Work Unit 34

11. CONTROLLING OFFICE NAME AND ADDRESS

Technology Branch, Turbine Engine Division (TBX)
Wright-Patterson AFB, Ohio 45433

12. REPORT DATE

January 1980

13. NUMBER OF PAGES

52

14. MONITORING AGENCY NAME & ADDRESS(if different from Controlling Office)

15. SECURITY CLASS. (of this report)

Unclassified

15a. DECLASSIFICATION/DOWNGRADING SCHEDULE

16. DISTRIBUTION STATEMENT (of this Report)

Approved for public release; distribution unlimited

17. DISTRIBUTION STATEMENT (of the abstract entered in Block 20, if different from Report)

18. SUPPLEMENTARY NOTES

19. KEY WORDS (Continue on reverse side if necessary and identify by block number)

Compressor aerodynamics
Rotor wakes
Radial flows

20. ABSTRACT (Continue on reverse side if necessary and identify by block number)

The detailed nature of the three-dimensional flow downstream of an isolated compressor rotor has been studied experimentally in a large scale rotating rig. Radial-circumferential arrays of pneumatic data have been acquired in the rotating frame of reference at values of (C_x/U_m) of 0.65, 0.75, 0.85 and 0.95 at planes 10, 30, 50 and 110% of blade axial chord aft of the rotor. The data consists of the total and static pressures and the

yaw and pitch angles. From this data the relative velocity vector has been completely defined. From the data it can be seen that the radial flow in the wake increases dramatically as the rotor loading is increased (by going to lower values of (C_x/U_m)). At high values of (C_x/U_m) low total pressure fluid accumulates at the hub causing corner stall. As (C_x/U_m) is reduced the radial flow carries the low total pressure fluid out to the tip, causing the hub corner stall to be inhibited, i.e. reduced in its streamwise extent aft of the blade trailing edge. By this process non-strip theory effects are seen to have a strong impact on the nature of rotor performance.

PREFACE

This report describes a contractual effort performed by the United Technologies Research Center for the Technology Branch (TBX) of the Turbine Engine Division (TB), Aero Propulsion Laboratory, Air Force Systems Command, Wright-Patterson Air Force Base, Ohio, under Project 2307, Task Sl, Work Unit 34.

The work reported herein was performed during the period 1 September 1977 to 30 September 1979 under the direction of C. Herbert Law (APL/TBX), project engineer, Contract Number F33615-77-C-2083. The principal investigator was Robert P. Dring of the United Technologies Research Center.

The authors are indebted to many people for the successful completion of this program and in particular to Mr. Hugh Hall and Mr. John Kostic for helping in acquiring the data, to Miss Diane Rodimon for reducing the data, and to the grace of God.

Accession For

NTIS GRA&I

DTIC TAB

Unannounced

Justification

By

Distribution/

Availability Codes

Dist | Avail and/or special

A

iii

Experimental Investigation of Compressor Rotor Wakes

TABLE OF CONTENTS

LIST OF ILLUSTRATIONS

LIST OF SYMBOLS

B	Airfoil true chord
B_x	Airfoil axial chord
C_p	Pressure coefficient: $(P_{T1} - P)/Q_{Um}$
C_x	Axial component of flow velocity
H	Boundary layer shape parameter: (δ^*/θ)
P	Pressure
P_{T1}	Inlet absolute total pressure
Q_{Um}	Dynamic pressure based on midspan wheel speed : $\left(\frac{1}{2} \rho U_m^2\right)$
t	Airfoil Thickness
U_m	Wheel speed at midspan
V	Flow velocity in the rotating frame
W	Wall static pressure
X	Axial distance
β^*	Airfoil metal angle (measured from tangential)
δ^*	Boundary layer displacement thickness
θ	Boundary layer momentum thickness
θ	Yaw (from axial direction, positive in direction of rotation)
ϕ	Pitch (positive away from rig axis)
ρ	Fluid density

Subscripts

R   Radial component (positive away from rig axis)

S   Static

T   Total

T   Tangential component (positive in direction of rotation)

X   Axial component

Superscripts

—   Pitch averaged

        Deviation from pitch average: $(V' = V - \bar{V})$

SECTION I

INTRODUCTION

In the design and analysis of any compressor one of the crucial flow analyses that is carried out is the streamline, or through-flow calculation. This is an axisymmetric meridional plane (two-dimensional) calculation in which the impact of the spanwise (or radial) variation of the flow properties is determined. The basic assumption common to all such calculations is that of strip theory. This is the assumption that adjacent streamtubes (or strips) communicate only through pressure gradients and that there is no transfer of mass, momentum or energy between them. In two-dimensional external flows this is generally an excellent assumption since the flows are usually homenthalpic and homentropic. In the internal flow in a compressor annulus, however, the flow is normally nonuniform. There are usually present large spanwise gradients in total pressure, total temperature and flow direction. These non-uniformities may be present in the inlet flow and they are also generated within, by the airfoils. Furthermore, the compressor annulus contains a host of mechanisms which contribute to the redistribution and mixing of these properties. These mechanisms include the radial flows in airfoil boundary layers and wakes, and the strong streamwise vortices generated by secondary flows at the endwalls and by rotor tip (and cantilevered stator root) clearance leakage flows. Furthermore, the same mechanism that causes radial flows in airfoil boundary layers and wakes, that is, differences in the absolute swirl velocity between fluid in the boundary layer or wake and the fluid around them, also causes these vortices to be transported radially.

An understanding of these non-strip theory effects would have a significant positive impact on the design and analysis of all axial compressor (and turbine) configurations. The impact, however, would be felt most strongly in the case of advanced technology compressors having low aspect ratio airfoils with high aerodynamic loading. The low aspect ratio causes the effects to be felt more strongly over a larger portion of the span. The high loading causes deeper wakes and stronger vortices which would result in higher radial velocities.

The present state-of-the-art in the area of through-flow calculations has been summarized at a recent AGARD conference (Ref. 1). In the Technical Evaluation Report it was stated that "the calculations schemes available....seem to have reached their maturity and to need only minor improvements." The observation was made that although the available numerics are probably adequate there is still a significant problem in the aerodynamic framework to which they are

1

being applied. Some of this problem is related to inadequate airfoil performance predictions but much of it must be directly related to non-strip theory effects in the annular flows. At present these effects are usually ignored both in compressor (and turbine) design calculations and in the through-flow analysis of rotating rig data. This is not surprising in light of the fact that there is very little available in the way of analytical models of the mechanisms and effects, and that only one or two pieces of data are available that even approach the degree of detail necessary to gain a clear picture of what is taking place.

Of the existing experimental studies in the area of rotor wake flows the most notable have been conducted by Thompkins and Kerrebrock (Ref. 2), Lakshminarayana and his coworkers (Refs. 3, 4 & 5), Hirsch et al (Ref. 6) and by Kool et al Ref. 7). The work by Thompkins et al (Ref. 2) was carried out behind a high speed rotor (M_{tip} = 1.2) using a radially traversing (nonrotating) multielement high response pressure probe. They measured the radial-circumferential distribution of total and static pressure and three components of velocity. It was observed that "very large radial flows, of the same order as the axial flow, occur in the flow field" thus indicating the potentially important role played by radial flow phenomena. The work by Raj et al (Ref. 3) also involved radially traversing a multielement high response sensor in the absolute (nonrotating) frame. In this case, however, a three element hot wire probe was employed. Close to the rotor trailing edge radial velocities of 10 to 15 percent of the axial velocity were measured in the very low work turbine configuration tested. The work by Reynolds et al (Ref. 4) employed a three element hot wire anemometer mounted in both the rotating and stationary frames of reference. Measurements were also made with a static pressure probe in the rotating frame of reference. Asymmetric profiles of radial flow in the wake were observed. The magnitude of these velocities was very large in the near-wake region and decayed rapidly with distance. Ravindranath (Ref. 5) also used a rotor mounted three element hot wire probe in his study of (moderately loaded) compressor rotor near and far wake behavior. A rotating frame "static-stagnation" probe was used to measure static pressure gradients. Measurements were made at several radial and axial locations. Once again, asymmetric radial velocity profiles of large magnitude were observed which decayed rapidly with distance. Hirsch et al (Ref. 6) examined the three-dimensional flow downstream of a compressor rotor using single element rotating hot wire instrumentation with phase-locked-averaging. Large radial flows were observed, especially near the rotor tip. Kool et al (Ref. 7) also used a rotating single element hot wire to obtain a complete plane of velocity component data. The data was taken 34 percent chord aft of a compressor rotor trailing edge and covered nearly the full span. The results showed the nature of the airfoil wakes, the endwall flow and local regions of large radial flow.

In a recent analytical work Sehra et al (Ref. 8) described a method for introducing nonaxisymmetric effects, including radial flow effects, into through-flow calculations. The approach is one of pitchwise averaging the equations of

motion rather than simply assuming axisymmetry. Some of the additional terms
arising as a result of this approach were demonstrated to have a significant
effect on obtaining agreement between measured and computed results.

The global objective of the present program was to make detailed measure-
ments which would determine the degree to which the assumption of strip theory
was being violated in the flow downstream of a compressor rotor. The specific
means whereby this was to be accomplished was by measuring the total and static
pressures and the three components of the flow velocity vector over a radial-
circumferential array in the rotating frame at several planes downstream of a
compressor rotor.

PROGRAM BACKGROUND

Since the probe is such a key feature of the program, its design and calibration will be described in detail. The combination 5-Hole/Cobra probe is shown in Fig. 1. The tip of the 5-Hole sensor (lower sensor) is on the shaft axis so that as the probe is rotated in yaw the sensor location will be fixed. The tip of the Cobra sensor (upper sensor) is also on the shaft axis for the same reason. The 5-Hole sensor can be positioned radially from a location very close to the outer case of the compressor (97% span) to a location approximately 3/4 inch from the rotor hub (13% span). The Cobra sensor was added in order to provide additional data down to approximately 1/4 inch from the rotor hub (4% span). The yaw and pitch angles for the probe are shown in the figure. This notation was used in the calibration results presented in Figs. 2 and 3. In the actual test, however, with the probe shaft coming radially out from the rotor hub the directions of yaw and pitch will be of opposite sign. Pitch will be positive in the radially outward direction and yaw will be positive in the direction of rotor motion. These sign conventions are included in the data reduction calculation.

The notation for the total of eight sensor pressure taps is shown in Fig. 1. For the Cobra sensor tap 1 is for impact pressure while taps 2 and 3 are for yaw nulling and dynamic pressure. For the 5-Hole sensor tap 5 is for impact pressure while taps 7 and 8 are for yaw nulling and taps 4 and 6 are for dynamic pressure and pitch.

Probe calibration was carried out in an air jet issuing from 1.5 inch diameter nozzle. The jet was sufficiently large such that both the 5-hole and Cobra sensors could be calibrated simultaneously. Calibration was carried out at a typical flow speed of 187 ft/sec. This relatively high speed was used in order to reduce the effects of the fixed manometer reading errors (approximately $\pm$ 0.01 inches of water). This method is permissible owning to the insensitivity of the probe calibration parameters to flow speed. The calibration was performed by setting the probe at a particular pitch, nulling the Cobra taps 2 and 3 in yaw, reading the yaw position relative to a flag mounted on the shaft and reading the pressures on taps 1 through 3. The 5-Hole sensor was then yawed until taps 7 and 8 balanced (null) and then the probe yaw angle and the pressures on taps 4 through 8 were recorded.

Typical calibration results are presented in Figs. 2 and 3 in terms of the various dimensionless coefficients that are used in the data reduction calculation. For the 5-Hole sensor the pitch parameter (Fig. 2A) is monotonic and nearly linear over a broad range. The dynamic pressure parameter (Fig. 2B) and

5

the total pressure parameter (Fig. 2C) are smooth and well behaved. The varia-
tion in the yaw angle at which null occurs (Fig. 2D) varies nearly linearly and
by less than 2° over the entire range of pitch. Finally, the symmetry about a
pitch of 0° indicated little or no interaction between the 5-Hole and Cobra
sensors. The Cobra sensor results are shown in Fig. 3 as a function of pitch
to indicate that over a wide range ($\pm$ 15°) they are insensitive to pitch.
This is important since the Cobra does not sense pitch. Only the constant
values of the various dimensionless parameters at zero pitch are used in the
data reduction.

SECTION III

TEST FACILITY

The experimental program was carried out in the United Technologies Research Center's Large Scale Rotating Rig (LSRR). This facility is 5 ft. (1.52 m) in diameter and is shown with the 0.8 hub/tip ratio compressor rotor installed in Fig. 4. The rotating frame radial-circumferential traverse system and the combination 5-Hole/Cobra probe can also be seen. The probe can be seen more clearly in Fig. 5 where it is in the plane 10% chord aft of the rotor. At typical running conditions the shaft speed is 510 rpm. At this shaft speed the flow through the rotor is set to obtain the desired value of (C_x/U_m). The test range of (C_x/U_m) from 0.65 to 0.95 corresponds to an axial flow velocity (C_x) range from 78 f/s (24 m/s) to 114 f/s (35 m/s).

The airfoil true chord is 6 ins (0.15 m) and is constant with span. This results in an airfoil aspect ratio of 1.0 and a Reynolds number range (based on inlet flow speed at midspan) of 4.3×10^5 to 5.1×10^5. The details of the airfoil geometry are listed in Table 1. The axial chord of the airfoil at midspan is is 5 ins. (0.15 m). The axial locations of the planes at which traverse data was obtained were measured with respect to the airfoil midspan trailing edge location and normalized with the midspan axial chord, e.g., the probe in Fig. 5 is nominally 10% aft of the rotor $(\Delta X/B_x = 0.1)$ so the probe is 0.5 ins. (0.13 m) axially aft of the blade tailing edge at midspan. A cross section of the flow path is shown in Fig. 6 with the traverse plane in its 10% aft location. The location of the various flow path static pressure taps and the location of the hub and tip inlet boundary layer surveys are also indicated. The rig flow (C_x) was based on the static pressure at Sta. 0 and the rotor pressure rise was based on the static pressure difference between Sta. 3 and Sta. 0. Note that the hub static pressure taps nominally at Sta. 0 are in fact 2 in. aft of Sta. 0. The traverse plane location relative to the rotor was varied by installing spacers between the traverse and the rotor. Thus, in order to traverse further aft of the rotor, the rotor and the nonrotating upstream hub were moved forward.

The rig is operated by a computerized automatic control, data acquisition and data reduction system. The system precisely maintains the desired velocity triangles by holding (C_x/U_m) to within $\pm 1/2\%$, calibrates all the various pressure transducers in the rotating and stationary frames, controls probe radial-circumferential positioning, acquires all penumatic data and reduces this data (on-line) to engineering units and convenient dimensionless parameters.

The accuracy of the pressure measurement system is typically $\pm 2\%$ of reading. Since all pressure measurements are referenced to the inlet absolute total pressure the uncertainty is $\pm 2\%$ of Cp.

SECTION IV

DISCUSSION

1. DATA PRESENTATION

Early in the program it was recognized that care would have to be taken in order to present the data in a form that would be useful to other investigators. Traverse data was taken at 4 axial planes and at four values of (C_x/U_m) in each plane. Measurements were made at roughly 900 radial-circumferential locations and each measurement consisted of 6 pieces of information (radial location, circumferential location, total pressure, static pressure, yaw and pitch). This adds up to over 80,000 pieces of information. It was determined that the most convenient method for storing such a bulk of information in an easily accessible form was on magnetic tape. For this reason, only a summary of the results will be presented in the following paragraphs. All of the data, however, is available on magnetic tape and the tape format is described in Appendix A.

In the following paragraphs the data is presented in the form of dimensionless pressure coefficients, normalized velocity components and flow angles. Both total and static pressures were referenced to the inlet absolute total pressure and the difference normalized by a dynamic pressure based on midspan wheel speed (Q_{U_m}). All of the velocity components were normalized with midspan wheel speed (U_m). Tangential velocity and yaw were taken as positive in the direction of rotor rotation (Fig. 6) and radial velocity and pitch are taken as positive in the radially outward direction. Circumferential location is increasing in the direction opposite to rotor rotation, i.e., from the pressure surface to the suction surface side of the wake (Fig. 6).

2. ROTOR PERFORMANCE

Two types of stationary frame data were acquired in order to document the overall rotor performance, the hub and tip inlet velocity profiles and the rotor static pressure rise characteristic. The inlet velocity profiles are shown in Fig. 7. Variation of C_x over the test range was seen to have no significant effect on the velocity profiles. The displacement and momentum thicknesses are about 1 to 2% of the blade chord (or span) and the boundary layer thickness is about 5 to 10% of the blade chord. The hub boundary layer is somewhat thinner than that at the tip. This is a result of the length of the hub centerbody being less than that of the flow path casing.

The rotor static pressure rise characteristic is shown in Fig. 8. The static pressure rise data from the hub and tip pressure taps (at Sta. 3, Fig. 6) are shown along with the deduced midspan static presure rise. For free-vortex

9

PRECEDING PAGE BLANK-NOT FILMED

swirl (and a 0.8 hub/tip ratio) the midspan static pressure is 58.3% of the way from the hub value to the tip value. This was the basis for estimating the mid-span static pressure rise. The data was taken with the rotor set up as in Fig. 6, i.e., with the traverse plane 10% aft of the rotor. The static pressure taps at Sta. 3 are then 200% (2 axial chords) aft of the rotor. This must be kept in mind when comparing these hub and tip static pressure data with those measured with the traverse probe. It will be seen that there is a considerable static pressure rise downstream of the rotor (probably resulting from wake mixing) and that the static pressure measured in the flow with the 5-Hole/Cobra probe does not extrapolate to the wall values until some distance aft of the rotor.

3. TRAVERSE DATA

The remainder of this discussion will provide a summary of the highlights of the radial-circumferential traverse data. The various pressure coefficients, nor-malized flow speeds and flow angles will be presented in a number of ways. Cir-cumferential plots are used to show the detailed nature of the flow in the wakes. Spanwise plots of the circumferentially gap (area) averaged results are used to show the data in a through-flow sense. Finally, in order to give an overall im-pression of the nature of the flow the data is presented in the form of contour plots.

Let us first examine the nature of the rotor wake flow at the plane 10% aft of the rotor trailing edge. The behavior of the blade wake at midspan is shown in Figs. 9 through 12 for (C_x/U_m) dropping from 0.95 to 0.65. This cor-responds to the midspan inlet flow angle (yaw) increasing from 46.4° to 57.0°, or the incidence going from -13° to -2.4°. At a (C_x/U_m) of 0.95 (Fig. 9) it can be seen that the maximum wake speed defect is about 30% and that the pitch variation is small ($\pm$ 2°) and asymmetric across the wake. As the flow (C_x/U_m) is reduced and the rotor loading increases, the maximum wake speed defect in-creases to about 70% at (C_x/U_m) = 0.65 (Fig. 12). The nature of the pitch distribution is also changing. The magnitude of the pitch angle in the wake is increasing (to over +30° at 0.65) and the distribution becomes nearly symmetric. As the rotor has been loaded up the wake has gone from having weak in and out flow ($\pm$ 2% of U_m at (C_x/U_m) = 0.95) to having a very strong radial out flow (+ 26% of U_m at (C_x/U_m) = 0.65). Clearly, airfoil loading has a strong impact of the magnitude of non-strip theory effects as a result of such flows.

It should also be pointed out that the measured variation in yaw (θ) across the wake also increased as (C_x/U_m) was reduced (from 2° at 0.95 to 27° at 0.65). Part of this may be a true yaw variation but part of it must be a result of the wake shear and the finite distance between the two nulling yaw parts on the probe (Fig. 1). As the probe moves across the wake from the pressure to the suction side of the wake the flow shear will first cause yaw error in the nega-tive direction in the region of dropping speed and then an error in the positive

direction in the region of increasing speed. It is expected that most of the measured yaw variation is due to this shear induced error since the yaw angles on either side of the wake are relatively close outside of the shear region. In future work of this sort it would be helpful to incorporate a first-order correction for this effect.

The spanwise distribution of the gap (area) averages is shown in Fig. 13 for a (C_x/U_m) of 0.65 (10% aft). The relative total pressure increases with span (due to the increase in wheel speed with span) out to 75%. Beyond this the tip leakage losses and the tip endwall boundary layer cause a rapid fall off. The beginning of the hub endwall effect is also apparent at 5% span. The static pressure increases monotonically with span but it is considerably below the hub and tip values (W) from the speed line (Fig. 8) which were measured 200% aft at Sta.3 (Fig. 6). It will be seen that at traverse planes further aft of the blade the static pressure rises toward these flow path values. This downstream diffusion is a result of wake mixing.

Even with the locally large values of pitch (Fig. 12) the gap averaged pitch is very small over most of the span except near the tip where it rises to +14°. The yaw variation is smooth, having significant over turning near the hub and under turning near the tip.

From the total and static pressure coefficients and the yaw and pitch one can calculate the various components of the velocity vector. These are shown (gap averaged) in Fig. 13. What is particularly noticeable is the large flow defect near the tip and that the gap averaged radial velocity is small even though there are locally very large radial flows (Fig. 12).

In order to check continuity of the measurements the area average of (V_x/U_m) was computed. This value should compare closely with the inlet value of (C_x/U_m), 0.65. The result must be corrected for inlet boundary layer displacement thickness and the extrapolation of traverse plane data to the hub and tip. These corrections are approximately 2% and they nearly cancel. The result was that the traverse plane exit flow exceeded the inlet flow by 2.7% for this case. This is rather good agreement, particularly in light of the strong gradients present in the flow this close to the rotor. This continuity check was carried out for all of the cases where it was possible. The average absolute error was 1.6% and the maximum error was 5%. This average error corresponds to a 1.6% error in speed (V/U_m) or a 2° error in the yaw angle. It is suspected that the major source of error was backlash in the traverse yaw positioning mechanism.

The contour plots of the various parameters provide an excellent picture of the flow. The total and static pressure coefficients, the flow speed and the yaw and pitch are presented in Figs. 14 through 18 respectively for (C_x/U_m) = 0.65, 10% aft. The primary endwall effect is at the tip (Fig. 14). The hub is

very clean. The static pressure is relatively uniform (Fig. 15) so the prime source of flow speed variation (Fig. 16) is the total pressure. The yaw angle gradients are relatively weak except in the wake where shear errors are greatest (Fig. 17). The radial flow (pitch) is seen to be almost entirely concentrated in the wake and in the region near the tip (Fig. 18). Note that the pitch data does not extend all the way to the hub due to the limited range of the 5-Hole sensor. The Cobra sensor doesn't sense pitch.

The nature of the flow field at the plane 10% aft was significantly different at values of (C_x/U_m) higher than 0.65. For these cases (0.75, 0.85 and 0.95) the region near the intersection of the airfoil and the hub had very low velocities and very large pitch angles. The data indicates that the blade was experiencing corner stall at the hub and that the region of back-flow extended to the plane 10% aft of the rotor. Because of the very low velocities and high pitches sensible data could not be obtained from either the Cobra probe or the 5-Hole probe when they were in this region. In order to learn as much as possible, however, data was acquired outside these apparently stalled regions. Data was not taken in the blade wake near the hub, however, it was taken in the regions between the wakes down to 4% span. The total pressure field is shown in Fig. 19 for the traverse plane 10% aft, at a (C_x/U_m) of 0.85. It is clear that the flow field is considerably different from that at the more highly loaded condition of a (C_x/U_m) of 0.65 (Fig. 14). At 0.85 the wake is much thinner, as could also be seen in Figs. 10 and 12. At the higher (C_x/U_m) there is a considerably smaller region of high loss fluid at the tip but there is a much larger region of high loss fluid at the hub. The reason for the breakdown in flow at the hub at higher values of (C_x/U_m) can be explained in part by the wake profiles of radial velocity (Figs. 9 through 12). At the higher values of (C_x/U_m) the endwall boundary layer fluid tends to accumulate on the airfoil near the hub. The radial flows in the wake (and probably also on the airfoil suction surface) are relatively weak so the low total pressure fluid accumulates there and causes the corner flow to break down. As the rotor is loaded up by going down in (C_x/U_m) to 0.65 the wake defect and the wake width (and the airfoil boundary layer thickness) increase. This permits the low total pressure fluid in the wake (and in the airfoil boundary layers) to be centrifuged radially outward (due to its high absolute swirl velocity). The effect is to remove the low total pressure fluid from the hub and to move it out toward the tip, thus inhibiting the hub corner stall, i.e., reducing the streamwise extent of the back-flow region. The final result is that due to non-strip theory effects, corner stall has been inhibited by increasing the loading on the rotor, i.e., by going to a lower (C_x/U_m).

The nature of the wake decay process is illustrated in Figures 19 thru 22. These figures show the total pressure fields at a (C_x/U_m) of 0.85 and at axial distances 10, 30, 50 and 110% aft respectively. At 10% aft (Figure 19) contours are shown near the hub between wakes but not in the wakes themselves. This is due to the inability of the probe to null in this apparently stalled region. By the traverse plane 30% aft (Fig. 20) it was possible to acquire data in all

12

parts of the wake. Upon examining the flow as it proceeds downstream it is clear that in both the airfoil wake and in the endwall regions, the total pressure (speed) defects are decreasing and that these regions of high loss fluid are increasing in extent. The process (at this C_x/U_m) appears to be primarily a diffusion process due to gradients rather than strong radial redistribution. The radial flow in most of the flow field is relatively weak (as mentioned above). The region of consistently highest pitch angle is near the airfoil wake in the vicinity of the hub.

The data has also been analyzed in the light of the observation by Sehra et al (Ref. 8) that blade-to-blade effects can have a significant impact on the results of through-flow calculations. The blade-to-blade effects are introduced into the through-flow analysis by circumferential averaging which produces the following terms: $\overline{V_X'^2}$, $\overline{V_R'^2}$, $\overline{V_T'^2}$, $\overline{V_X'V_R'}$, $\overline{V_X'V_T'}$, and $\overline{V_R'V_T'}$. For the supersonic rotor data analyzed in Ref. 8 these terms range in magnitude from -2% to +7% of $\overline{V_X2}$. The data of Ref. 8 showed very strong radial gradients over the entire span with no significant differences in magnitude between midspan flow and flow near the endwalls. In addition, there was no signficant change in the magnitude of the terms from 10 to 100% aft of their rotor.

The results of the present program were analyzed in this same way and are shown in Figs. 23, 24 and 25. The data of the present program have been normalized with midspan wheel speed. To convert them to percent $\overline{V_X'2}$ they must be multiplied by $(C_x/U_m)^{-2}$. This factor is 2.4 for a (C_x/U_m) of 0.65 and 1.4 for a (C_x/U_m) of 0.85. The data for (C_x/U_m) of 0.85 at 10% aft is shown in Fig. 23. The largest positive term is $\overline{V_X'^2}$ and the largest negative term is $\overline{V_X'V_T'}$. Large values occur near the hub and tip which are comparable in magnitude to those of Ref. 8. In the midspan region, however, the terms are all much smaller than those of Ref. 8. As the rotor is loaded up by going down to a (C_x/U_m) of 0.65 (Fig. 24) the terms increase in magnitude in the midspan region. Under these conditions their magnitudes even at midspan are on the order of those reported in Ref. 8. Further downstream at this same value of (C_x/U_m) the terms are generally of much smaller magnitude due to the wake mixing that has occurred aft of the rotor (Fig. 25). This is distinctly different from the behavior observed aft of the supersonic rotor of Ref. 8 where little change was observed with axial location.

SECTION V

CONCLUSIONS

It has been demonstrated that non-strip theory radial flow effects can
have a major impact on the nature of the wake of a compressor rotor. Rotating
frame radial-circumferential traverse data has shown that as the rotor loading
is increased, by reducing (C_x/U_m), the airfoil wake depth and width increase
and that at sufficiently high loadings very strong radial flow can occur (as high
as 28% of C_x). The result is that the accumulation of low total pressure fluid,
which resulted in a hub corner stall at lower loadings, is inhibited due to rad-
ial out flow at higher loadings. Non-strip theory effects such as these can have
a significant impact on compressor design and on the analysis of compressor rig
data.

TABLE 1

ROTOR AIRFOIL GEOMETRY

Contour – NACA 65 Series
Chord (B) – 6 ins. (0.1524 m.)
Camber – Circular Arc
No. of Airfoils – 28

Span (%)	0	25	50	75	100
β_1^* (deg.)	25.37	31.80	30.55	28.45	25.03
β_2^* (deg.)	104.77	85.75	78.50	74.45	74.47
t/B	0.0900	0.0825	0.0750	0.0675	0.0600
Radius(ins.)	24.0	25.5	27.0	28.5	30.0

16
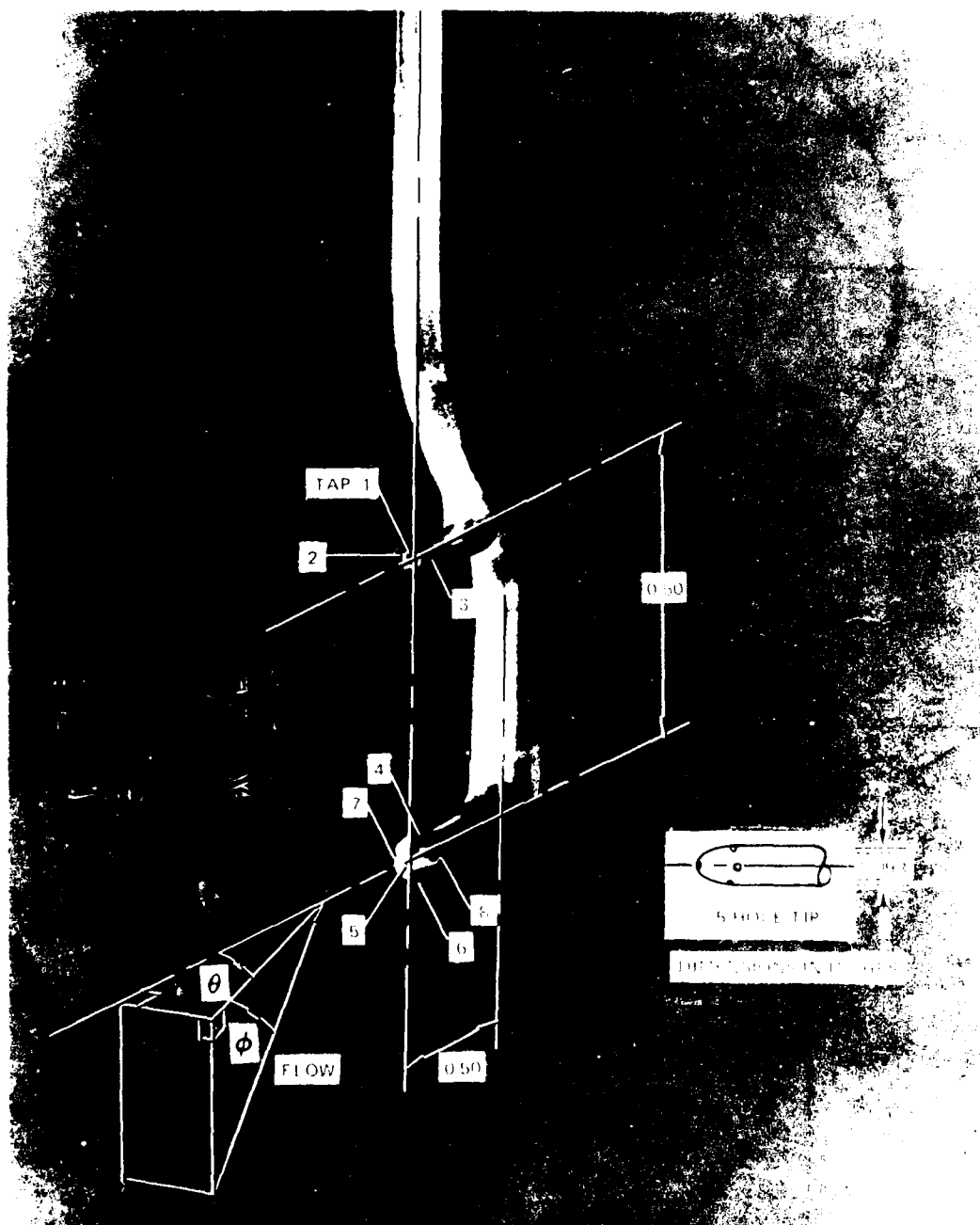
Figure 1. Combination Five Hole/Cobra Probe

17

CALIBRATION PARAMETERS

B

2.0
1.6
1.2
0.8
0.4

$[P5-(P6+P4)/2]/q$

D

3.0
2.0
1.0
0
-1.0
-2.0

θ CAL – DEG

-30   -15   0   15   30

A

3.0
2.0
1.0
0
-1.0
-2.0

$(P6-P4)/[P5-(P6+P4)/2]$

C

1.0
0.8
0.6
0.4
0.2
0

$[PT-P5]/q$

-30   -15   0   15   30

PITCH ANGLE, ϕ – DEG

$q = 7.61$ IN. H_2O $P_{bar} = 29.936$ IN. Hg $T_{cal} = 83.53\ ^\circ F$
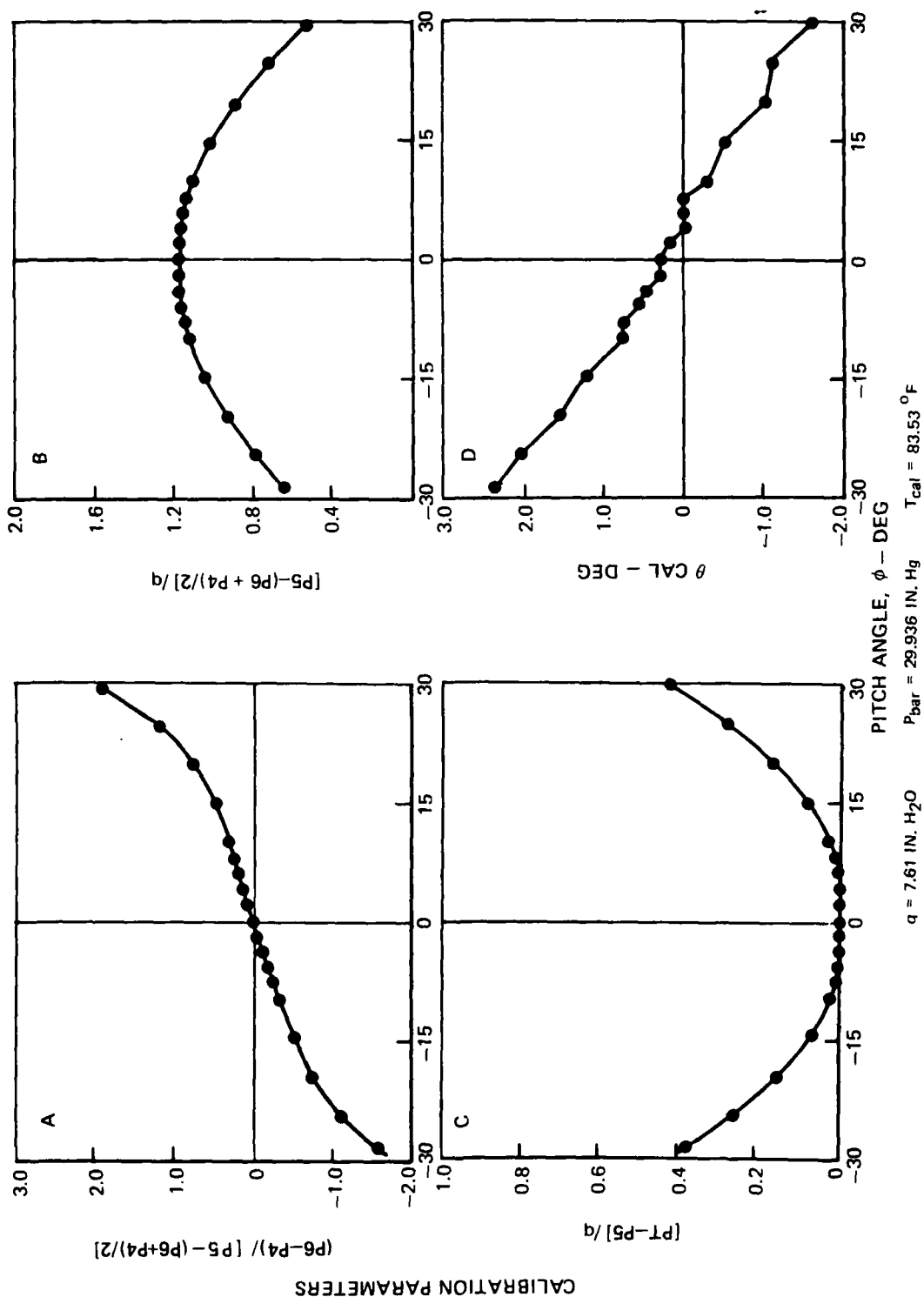
Figure 2. Typical Five Hole Probe Calibration

18

$q = 7.61$ IN H_2O

$P_{bar} = 29.936$ IN. Hg

$T_{cal} = 84.53\ ^\circ F$

A

$(P1-P2)/q$

B

$(PT-P1)/q$

C

$\theta\ CAL - DEG$

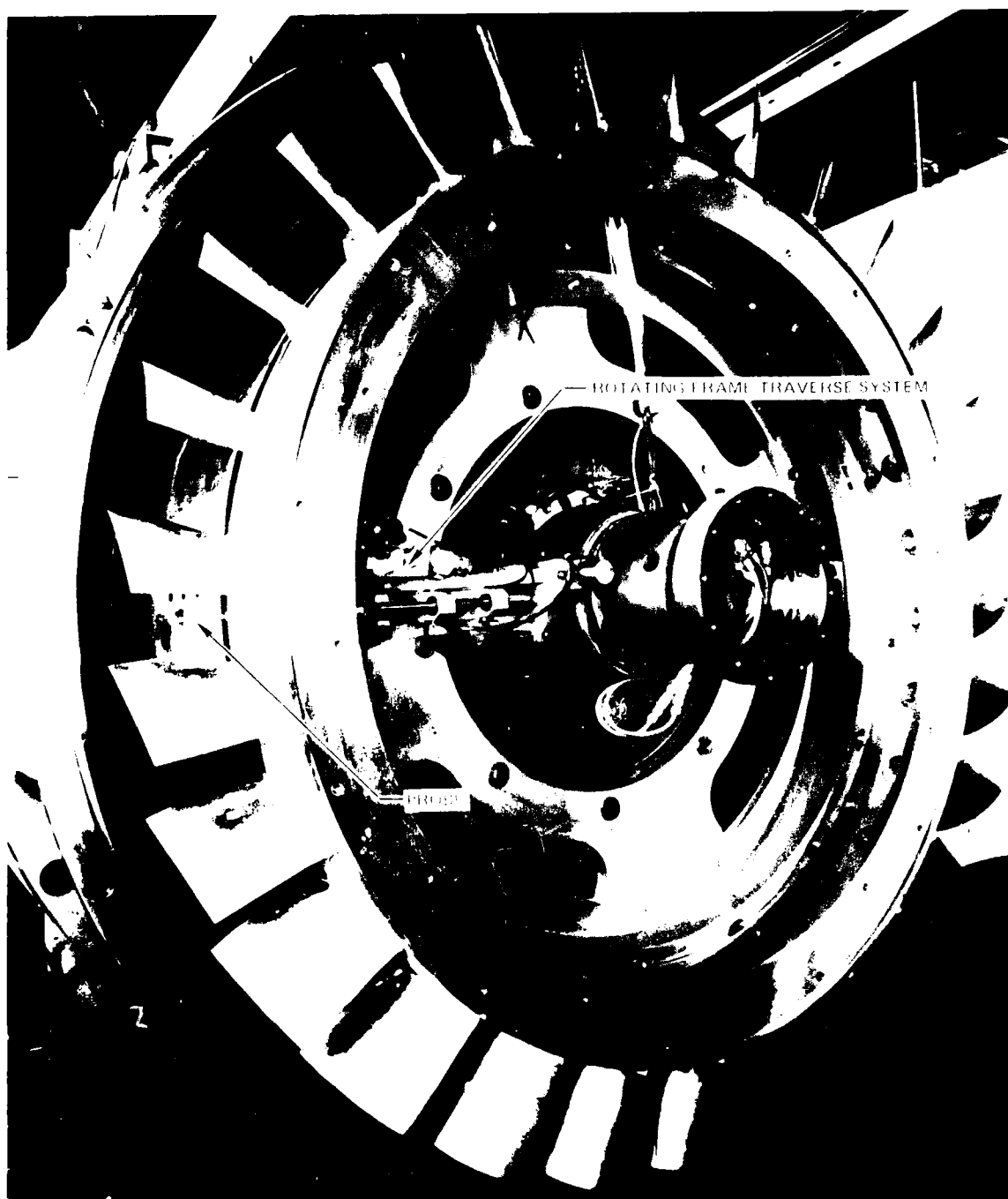PITCH ANGLE, ϕ - DEG
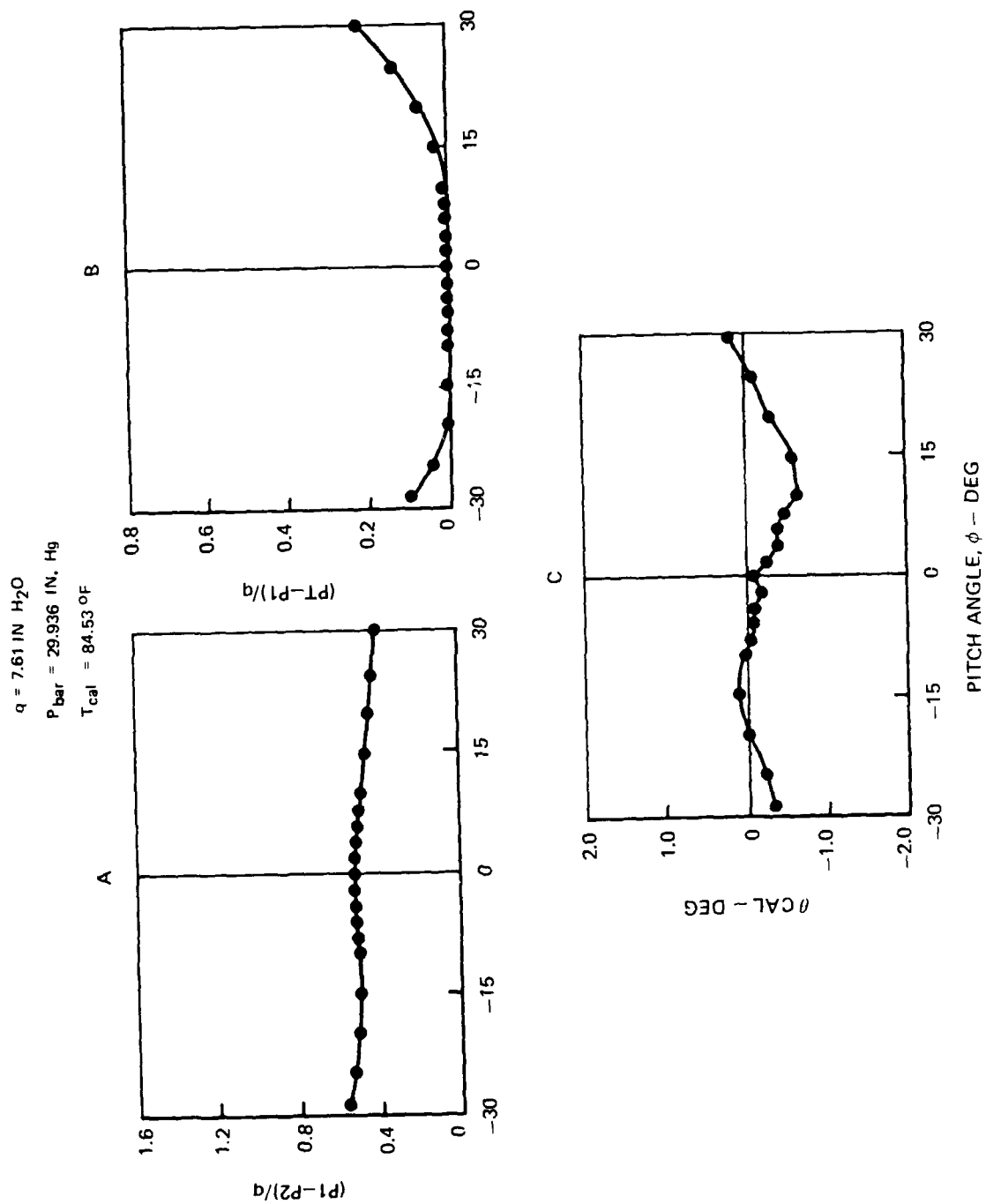
Figure 3. Typical Cobra Probe Calibration

Figure 4. Isolated Compressor Rotor With Rotating Frame Traverse System

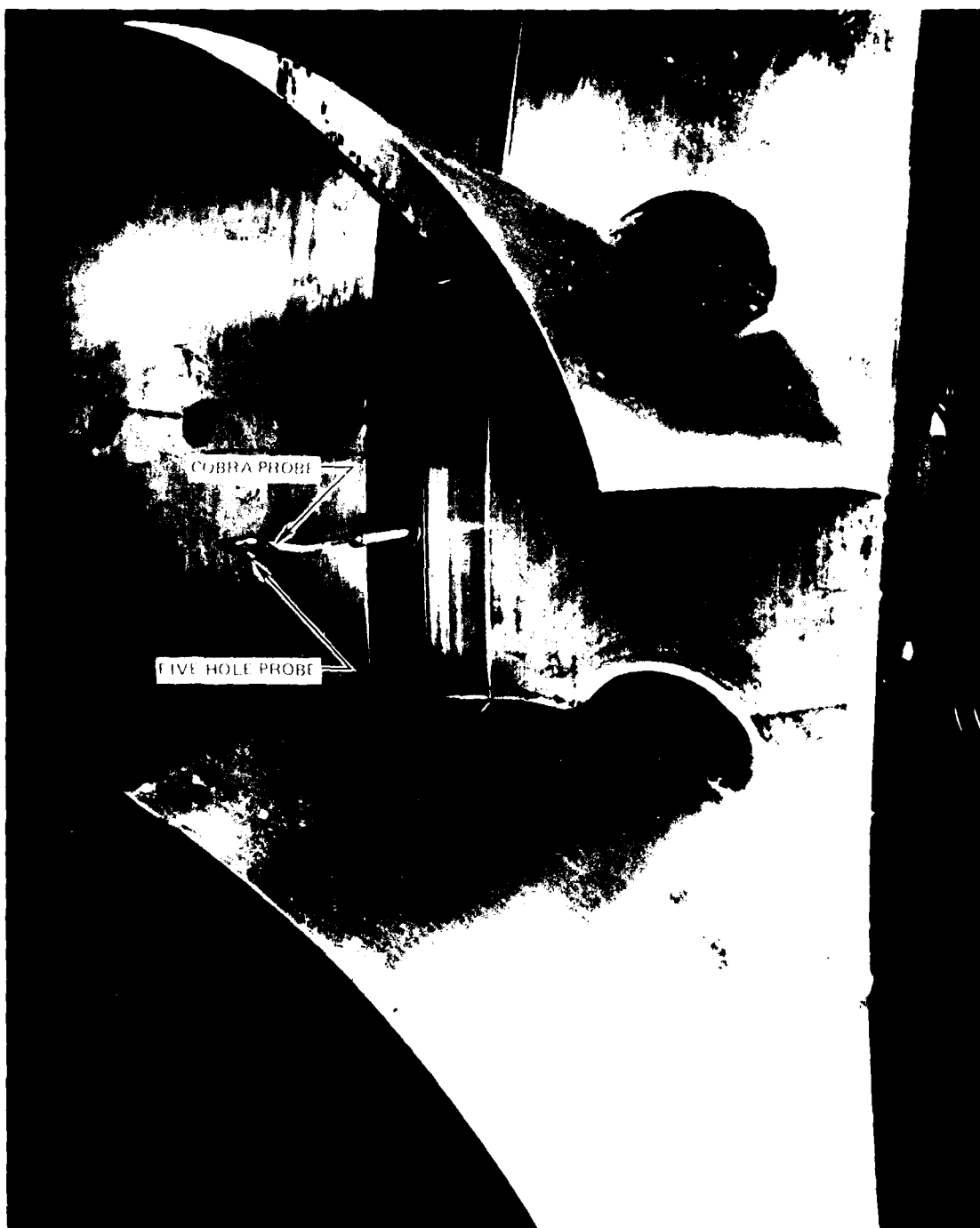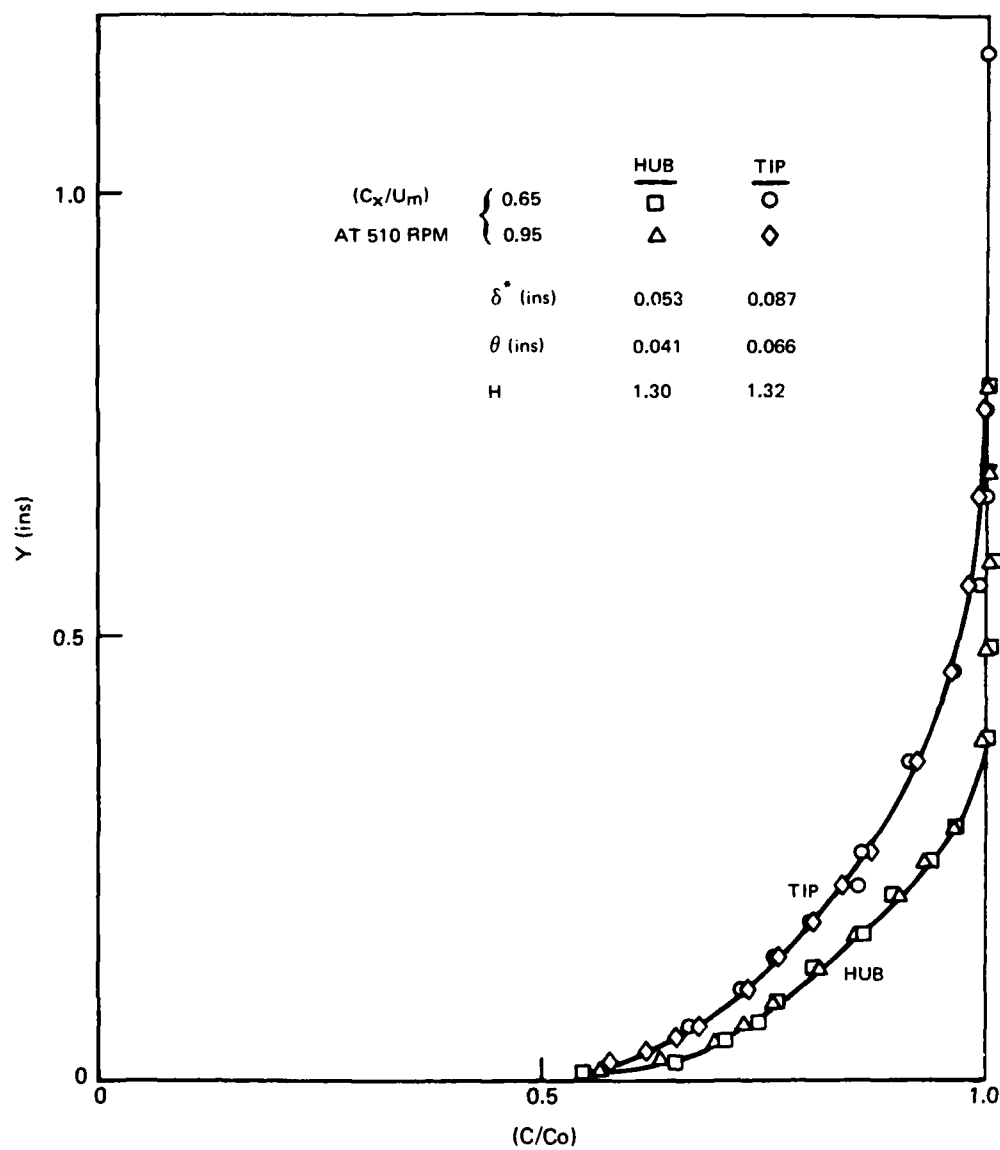Figure 5. Rotating Frame Combination Five Hole/Cobra Probe

21

Figure 6. Flow Path Schematic

22

Y (ins)

1.0

0.5

0

		HUB	TIP
(C_x/U_m)	0.65	□	○
AT 510 RPM	0.95	△	◇
δ^* (ins)		0.053	0.087
θ (ins)		0.041	0.066
H		1.30	1.32

TIP
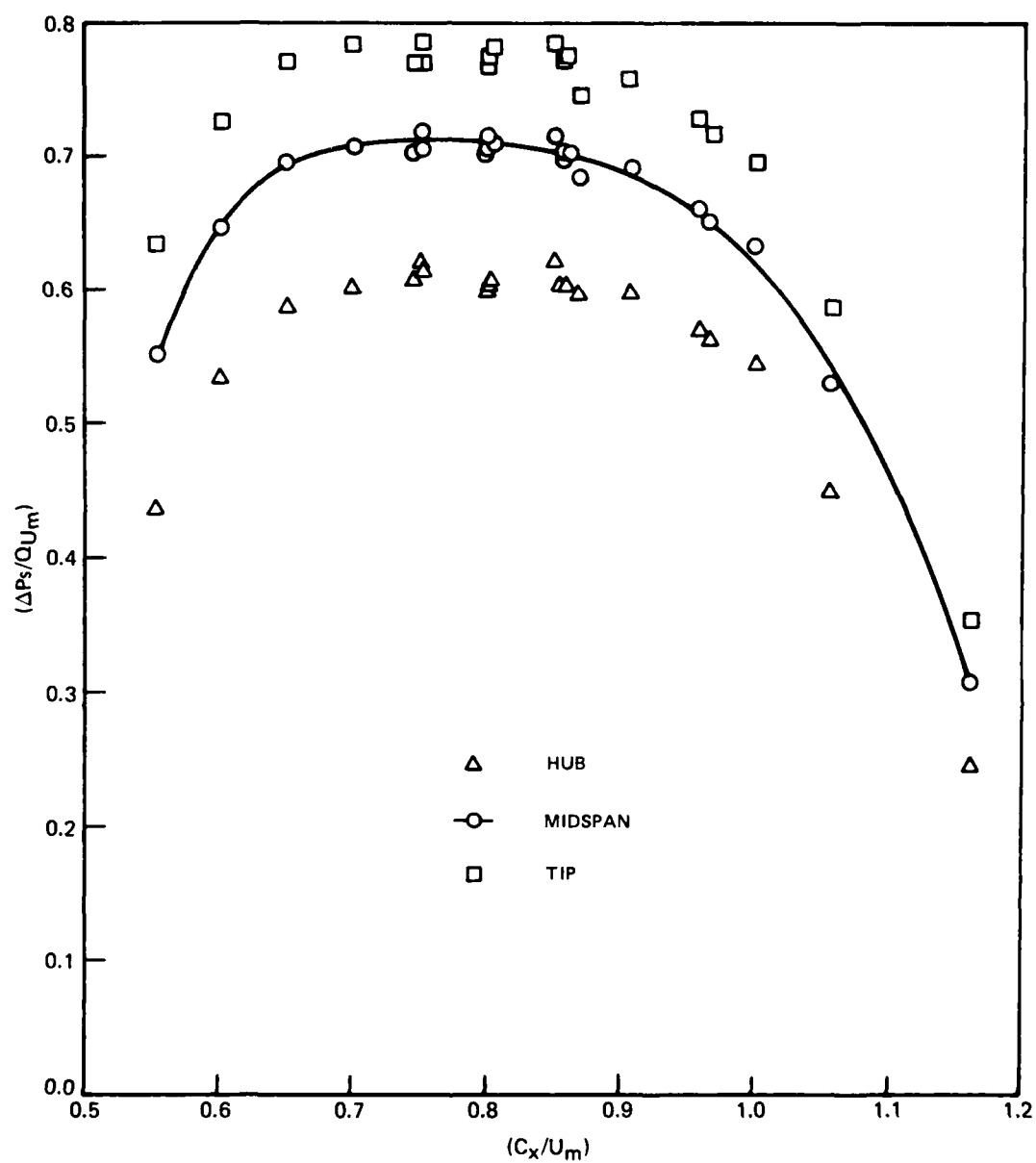
HUB

0   0.5   1.0

(C/Co)

Figure 7. Hub & Tip Inlet Boundary Layers

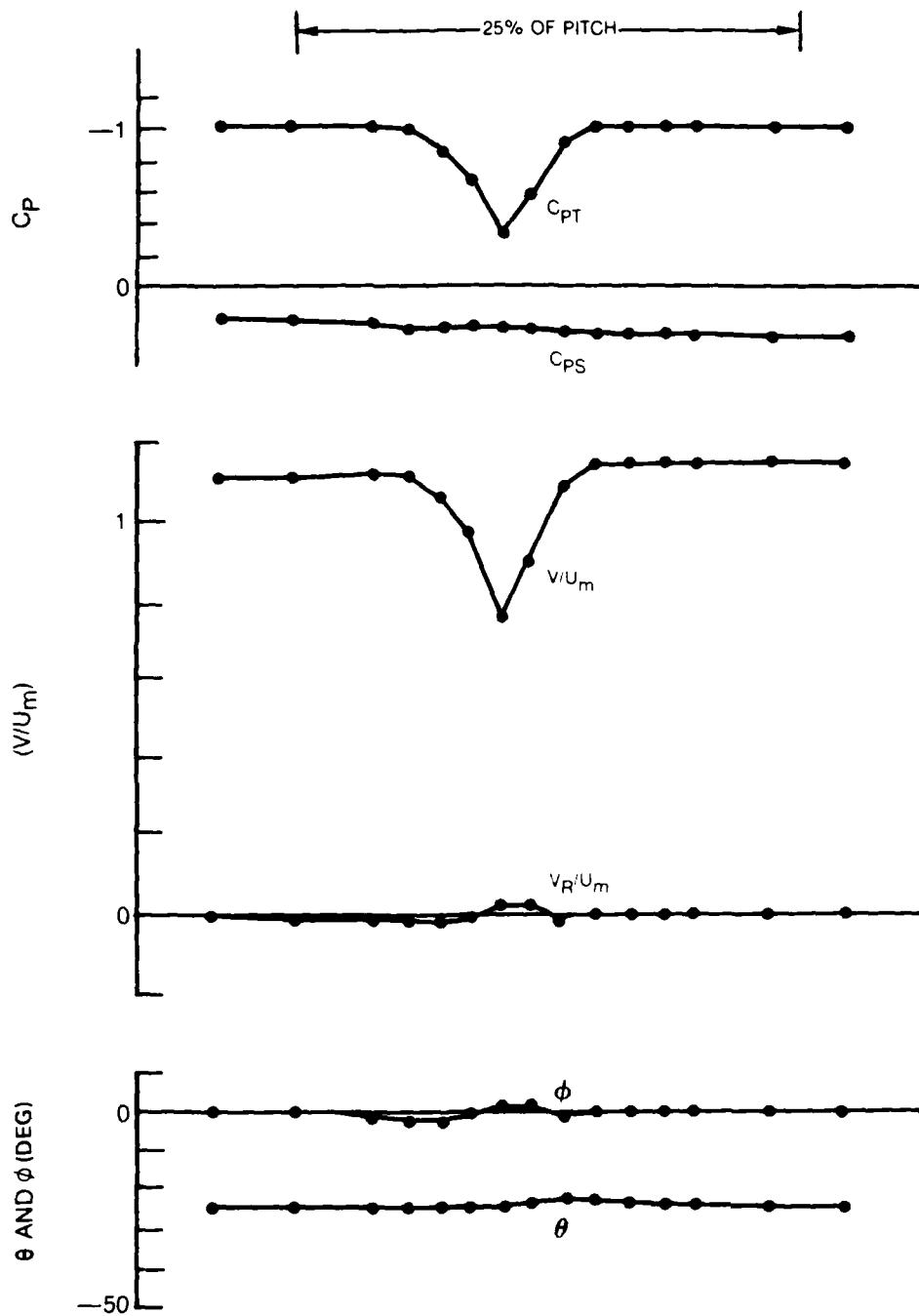Figure 8.   Isolated Rotor Static Pressure Rise

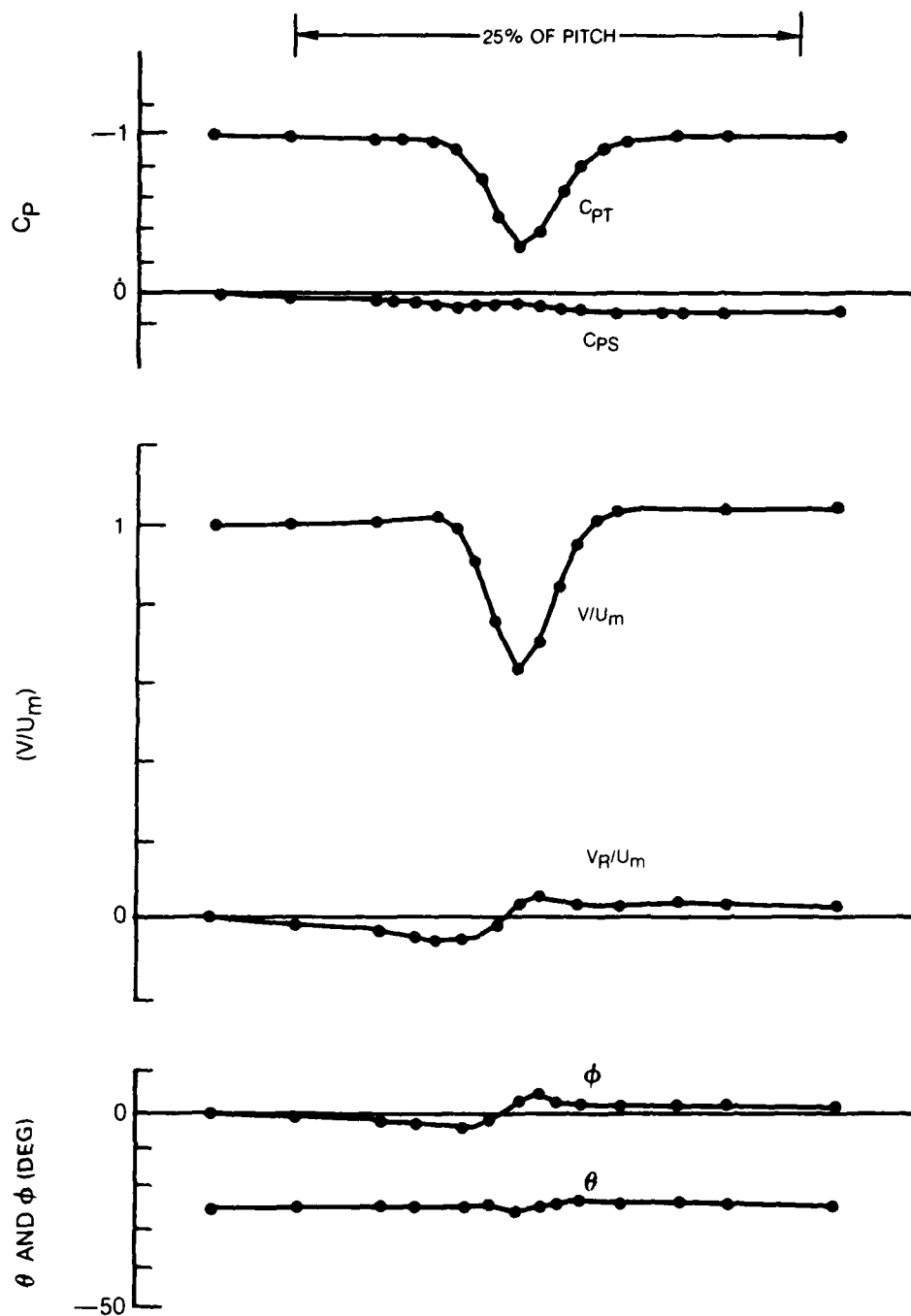Figure 9.   Midspan Rotor Wake, 10% Aft, $(C_x/U_m) = 0.95$

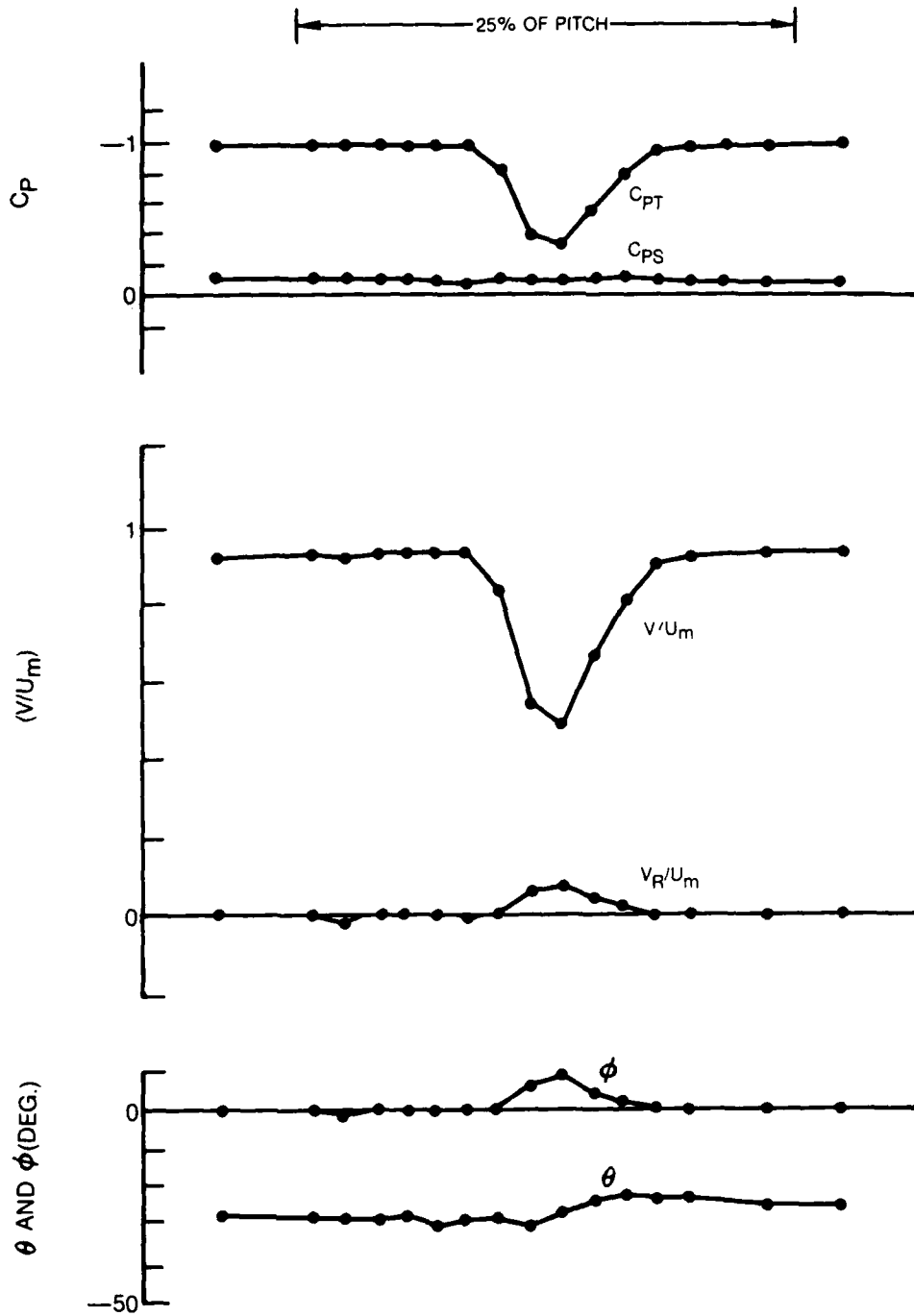Figure 10. Midspan Rotor Wake, 10% Aft, $(C_x/U_m) = 0.85$

26

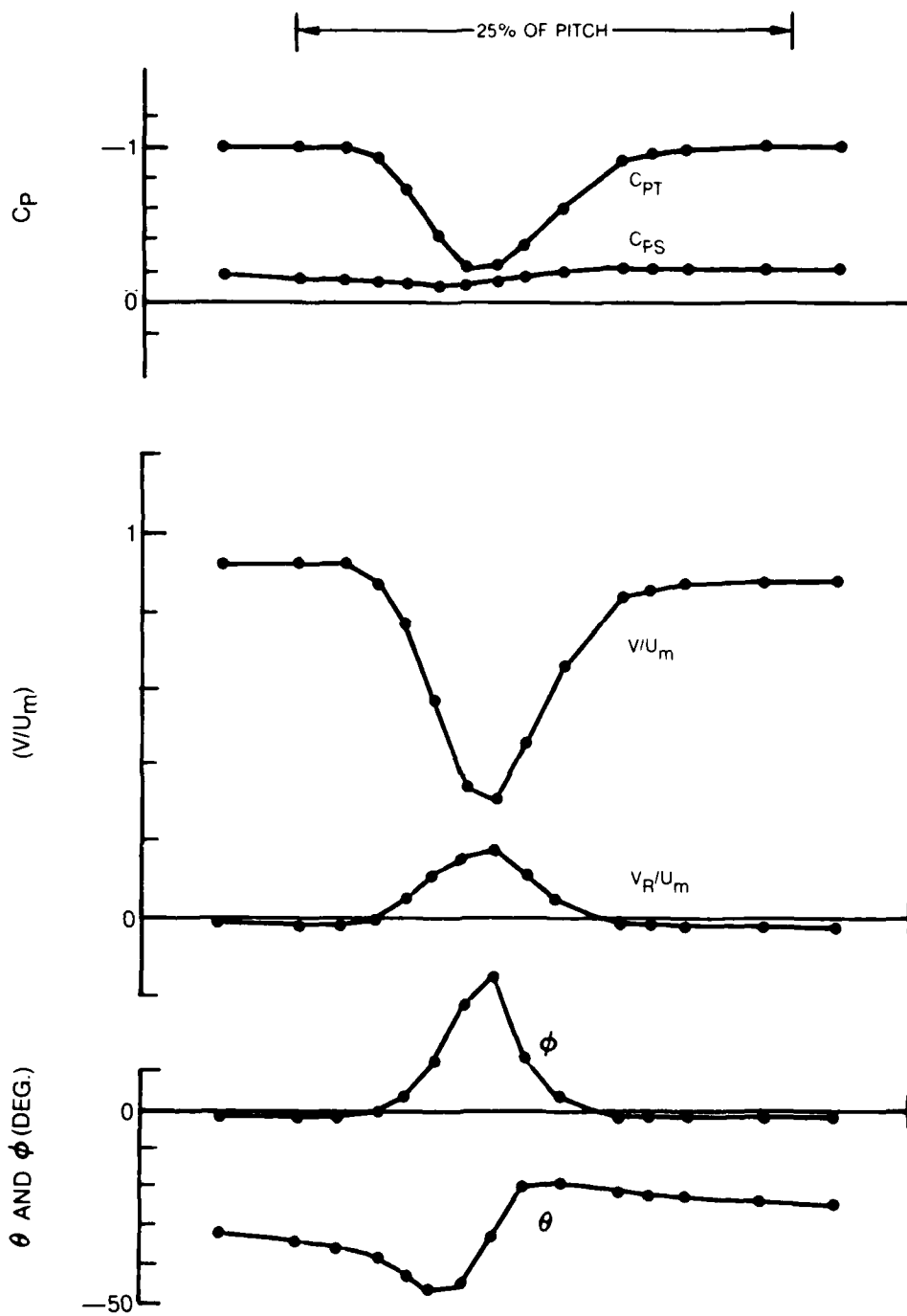Figure 11. Midspan Rotor Wake, 10% Aft, $(C_x/U_m) = 0.75$

Figure 12. Midspan Rotor Wake, 10% Aft, $(C_x/U_m) = 0.65$

28
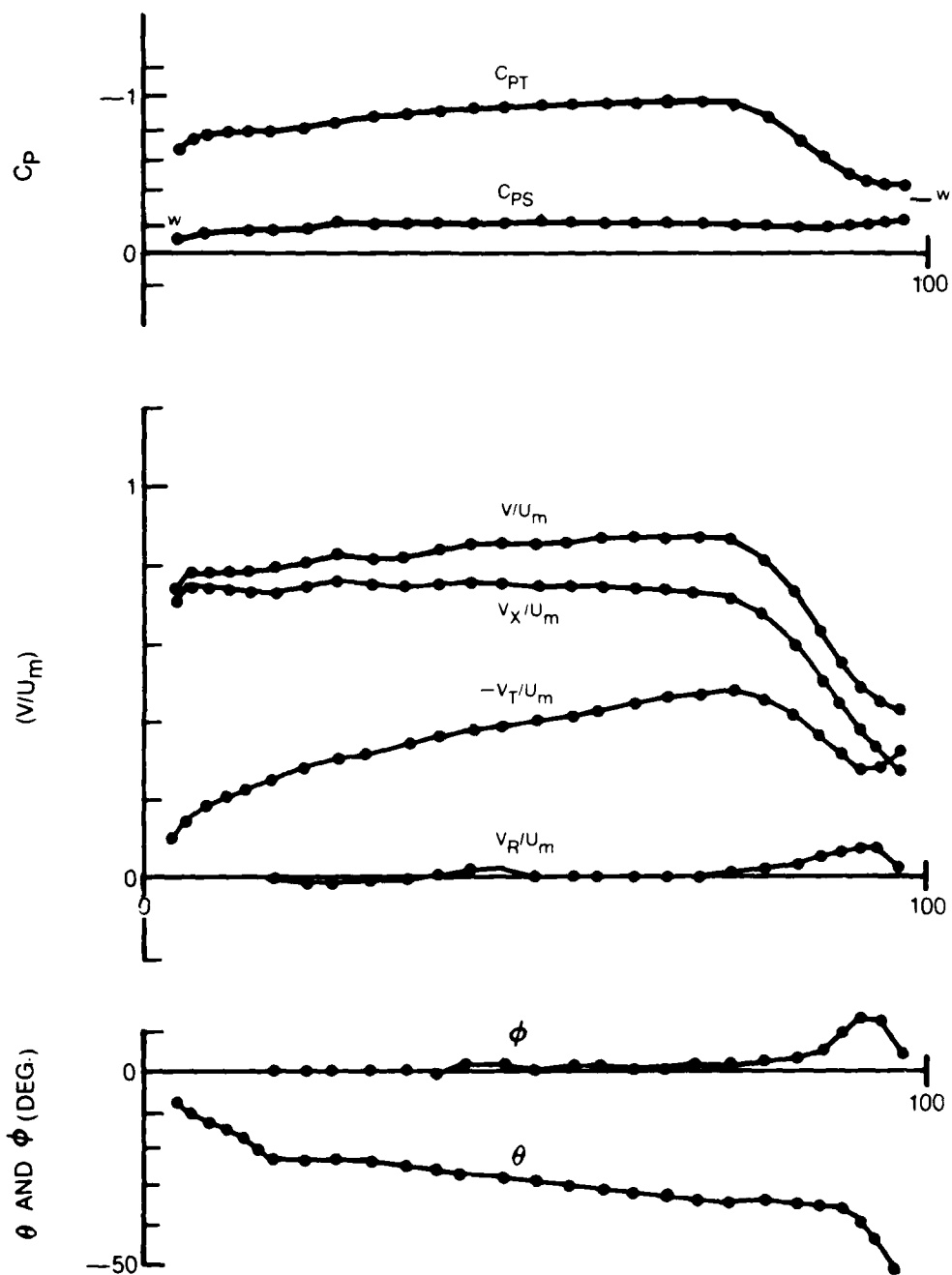
Figure 13. Spanwise Flow Distributions, 10% Aft, $(C_x/U_m) = 0.65$

1.56 PITCHES
CONTOUR INCREMENT:
$\Delta C_P = 0.1$

SUCTION SURFACE

PRESSURE SURFACE
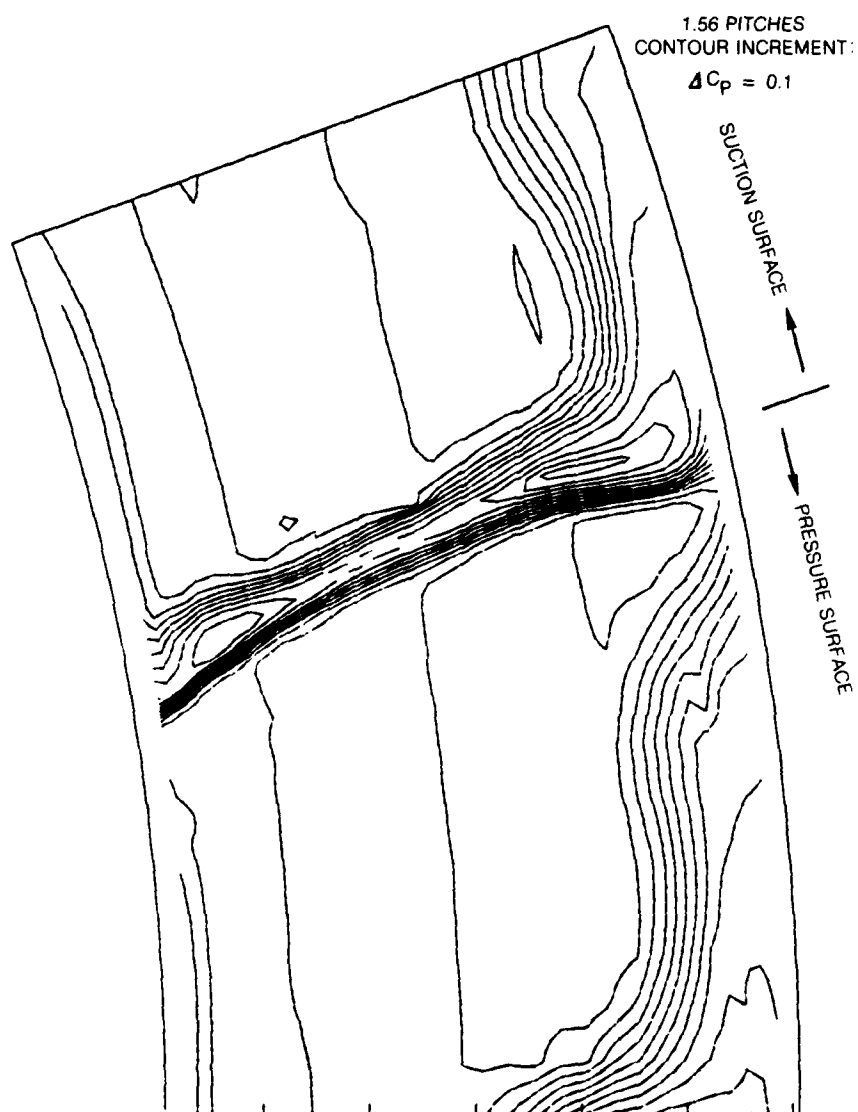
Figure 14. Total Pressure Contours, 10% Aft, $(C_x/U_m) = 0.65$

1.56 PITCHES
CONTOUR INCREMENT
$\Delta C_P = 0.1$
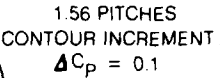
Figure 15. Static Pressure Contours, 10% Aft, $(C_x/U_m) = 0.65$

1.56 PITCHES
CONTOUR INCREMENT:
$\Delta(V/U_m) = 0.1$
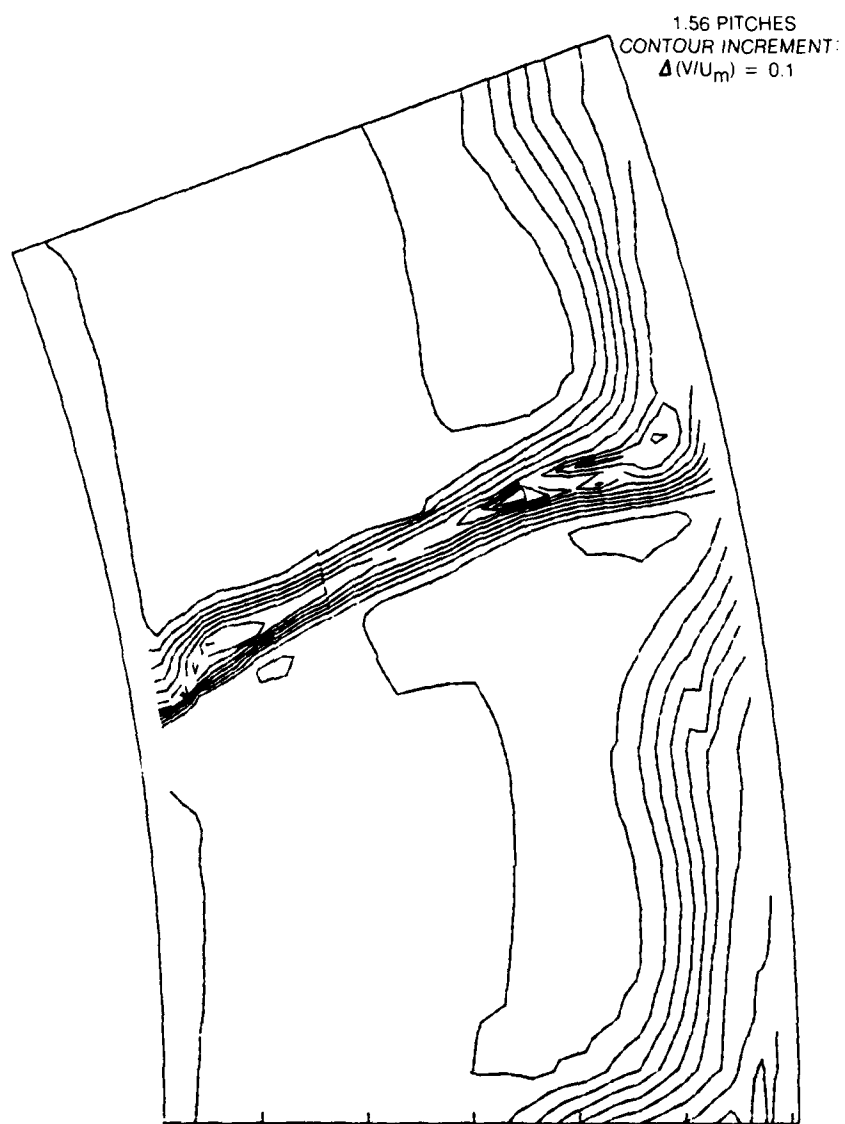
Figure 16. Flow Speed Contours, 10% Aft, $(C_x/U_m) = 0.65$

1.56 PITCHES
CONTOUR INCREMENT:
$\Delta\theta = 5°$
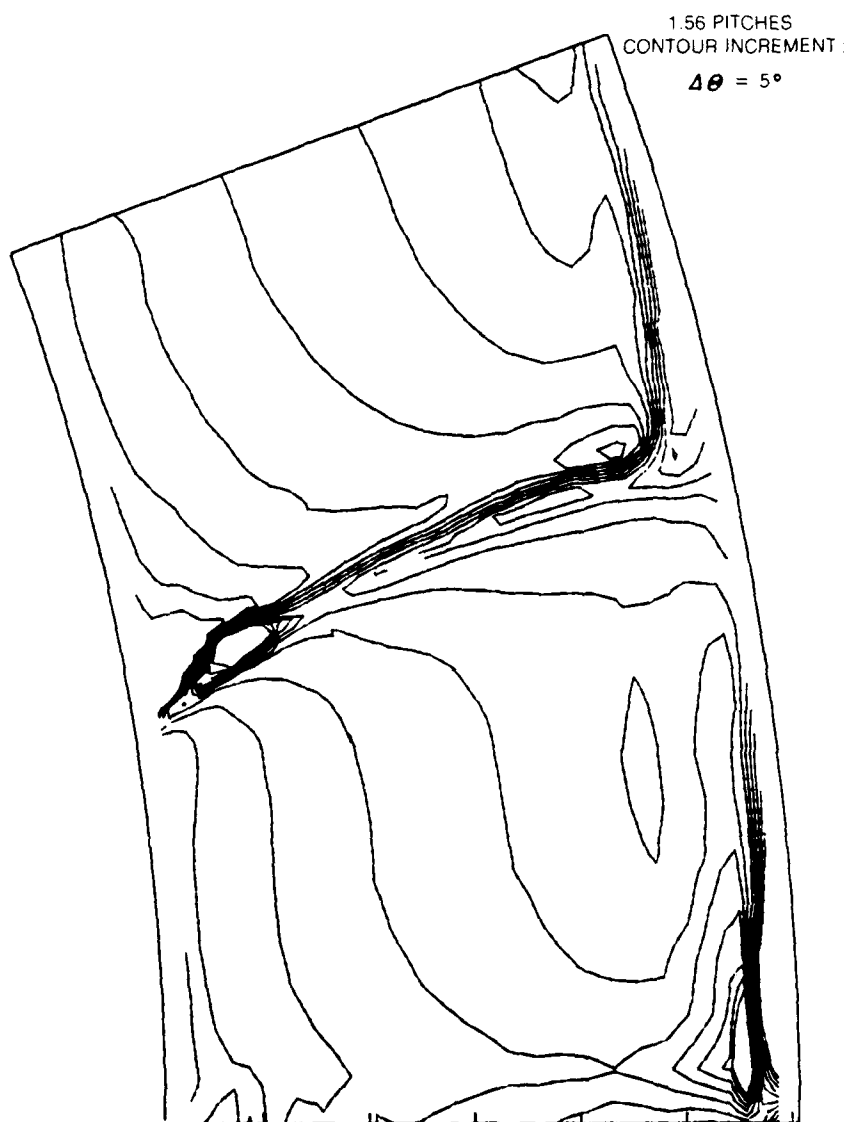
Figure 17. Yaw Contours, 10% Aft, $(C_x/U_m) = 0.65$
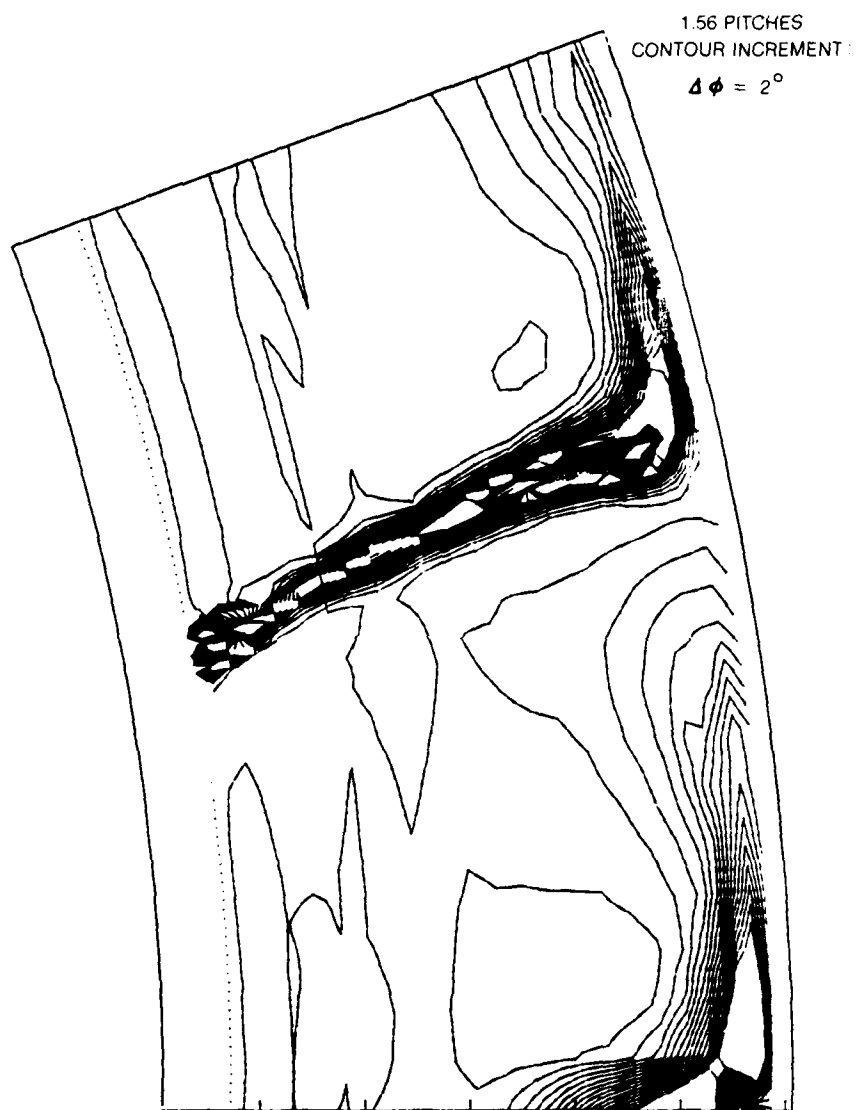
Figure 18. Pitch Contours, 10% Aft, $(C_x/U_m) = 0.65$

1.87 PITCHES
CONTOUR INCREMENT
$\Delta C_P = 0 1$
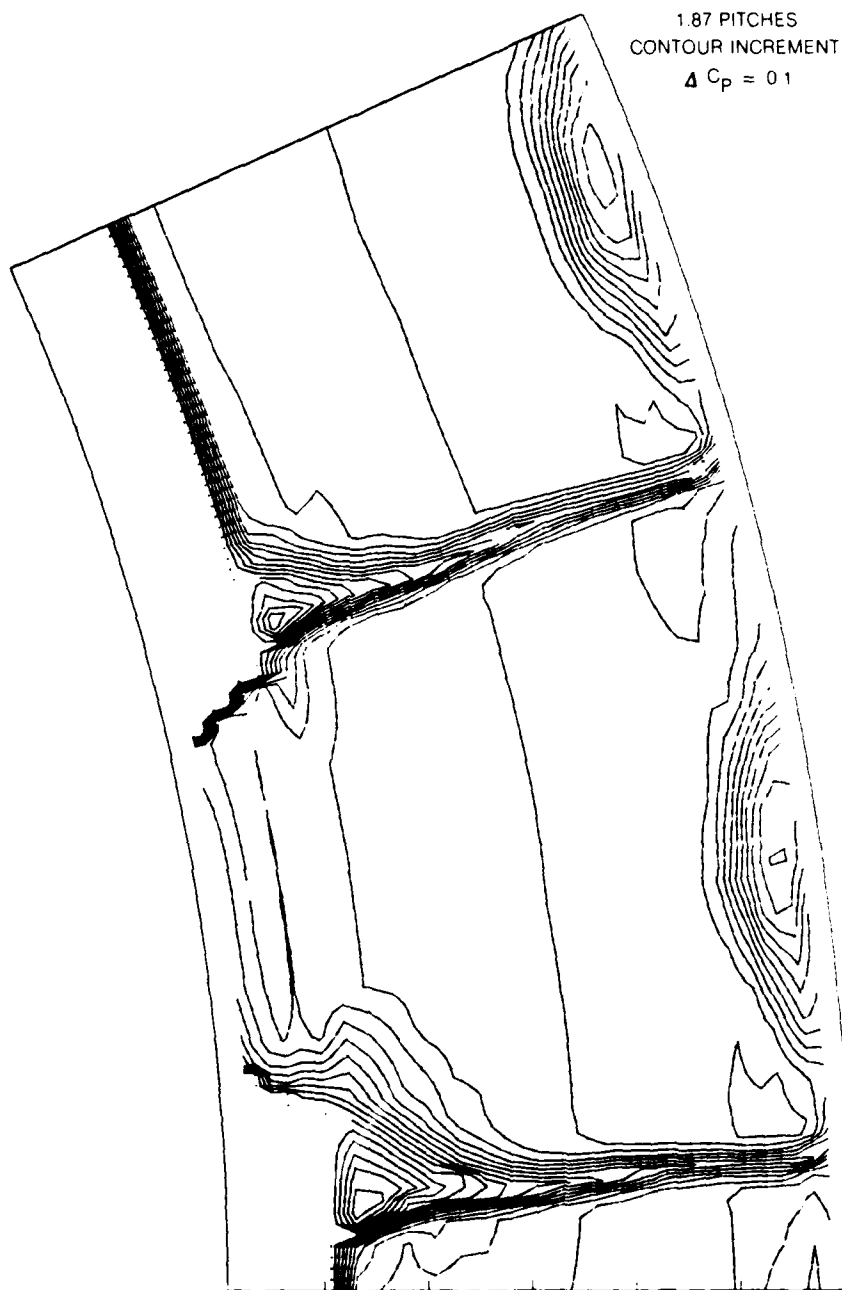
Figure 19. Total Pressure Contours, 10% Aft, $(C_x/U_m) = 0.85$

35

1 32 PITCHES
CONTOUR INCREMENT
$\Delta C_P = 0.1$
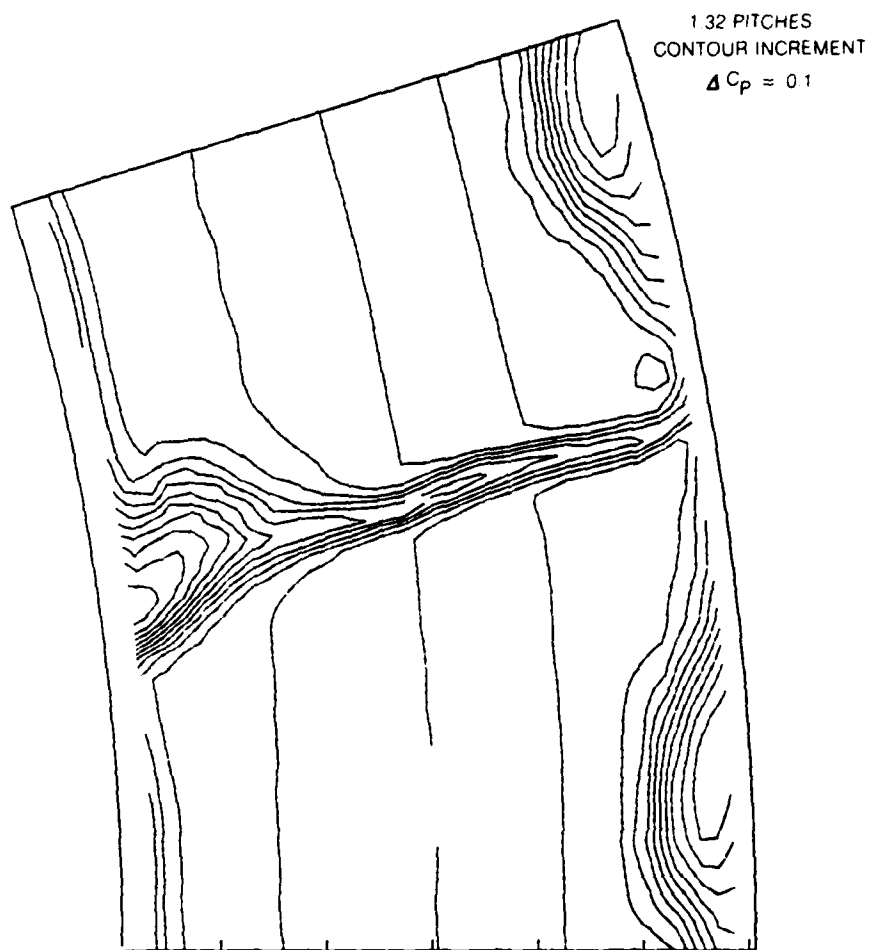
Figure 20. Total Pressure Contours, 30% Aft, $(C_x/U_m) = 0.85$

1.32 PITCHES
CONTOUR INCREMENT
$\Delta C_P = 0.1$
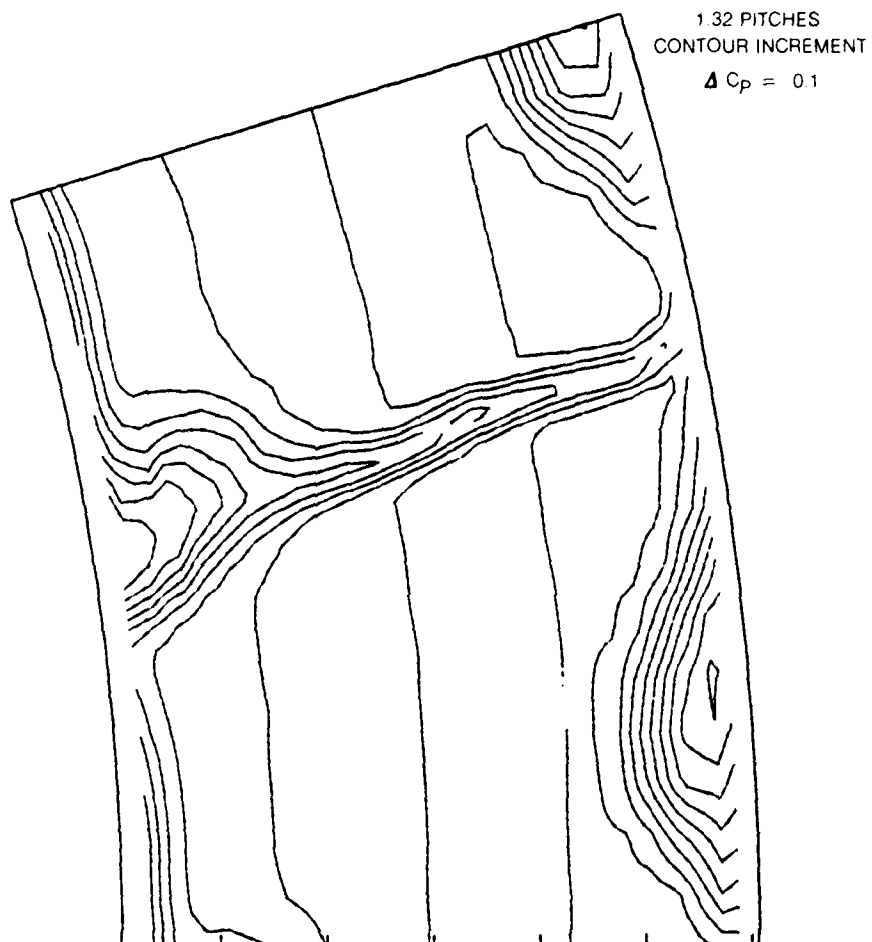
Figure 21. Total Pressure Contours, 50% Aft, $(C_x/U_m) = 0.85$

1.32 PITCHES
CONTOUR INCREMENT:
$\Delta C_P = 0.1$

Figure 22. Total Pressure Contours, 110% Aft, $(C_x/U_m) = 0.85$

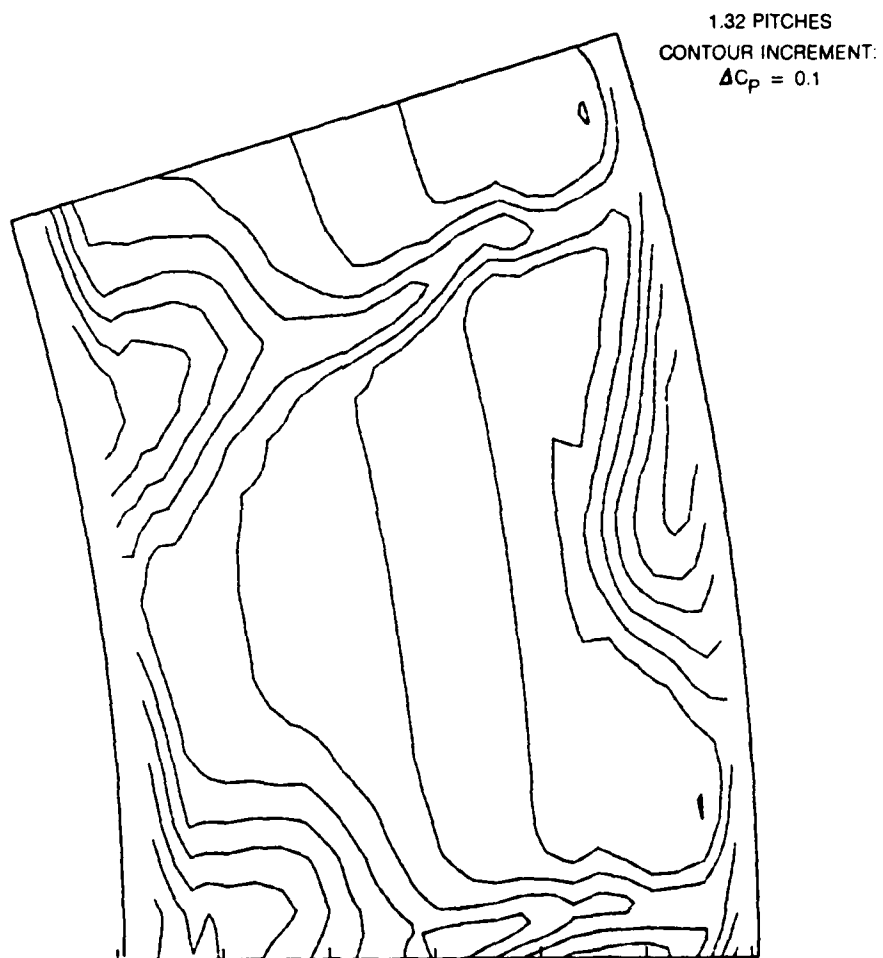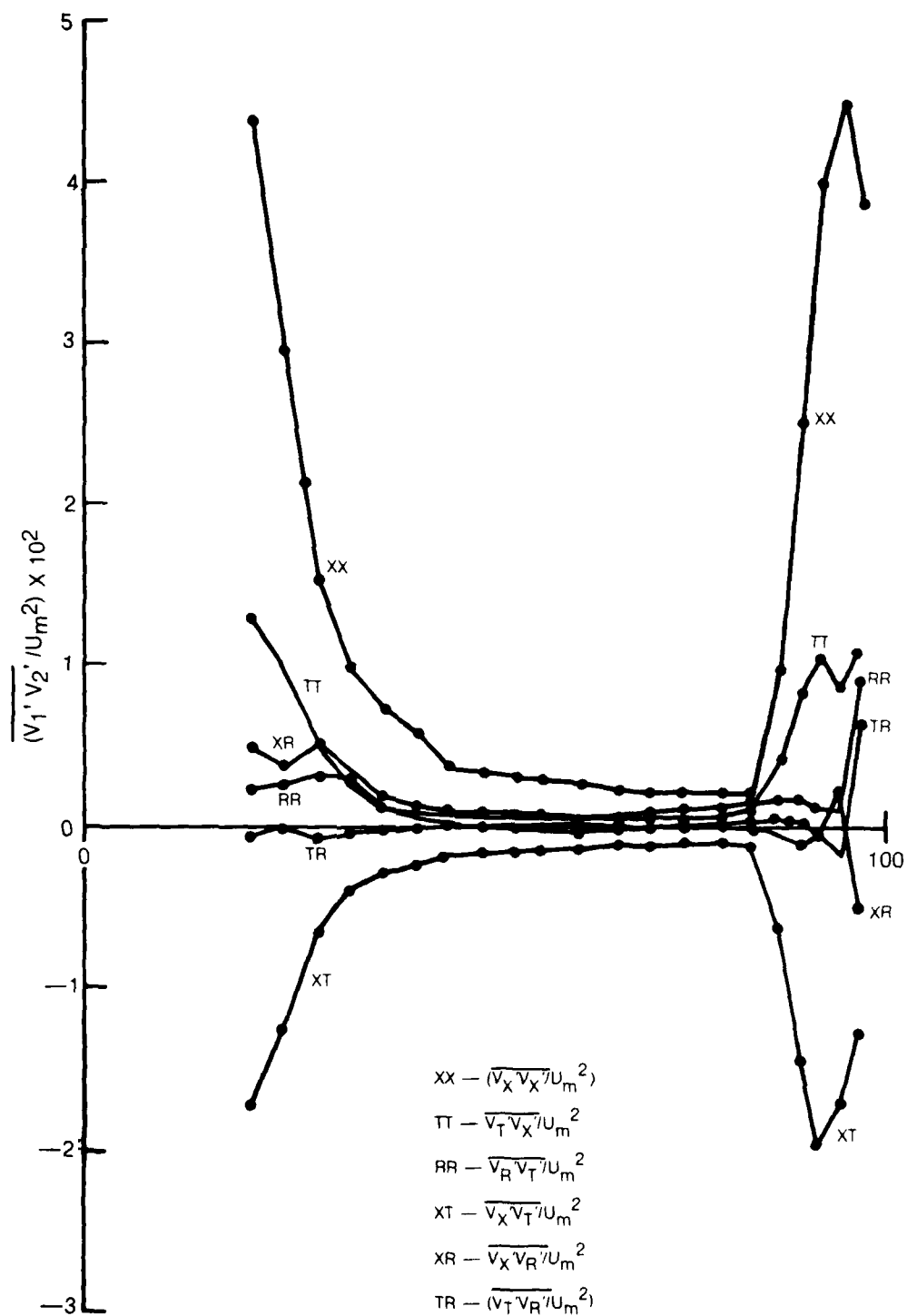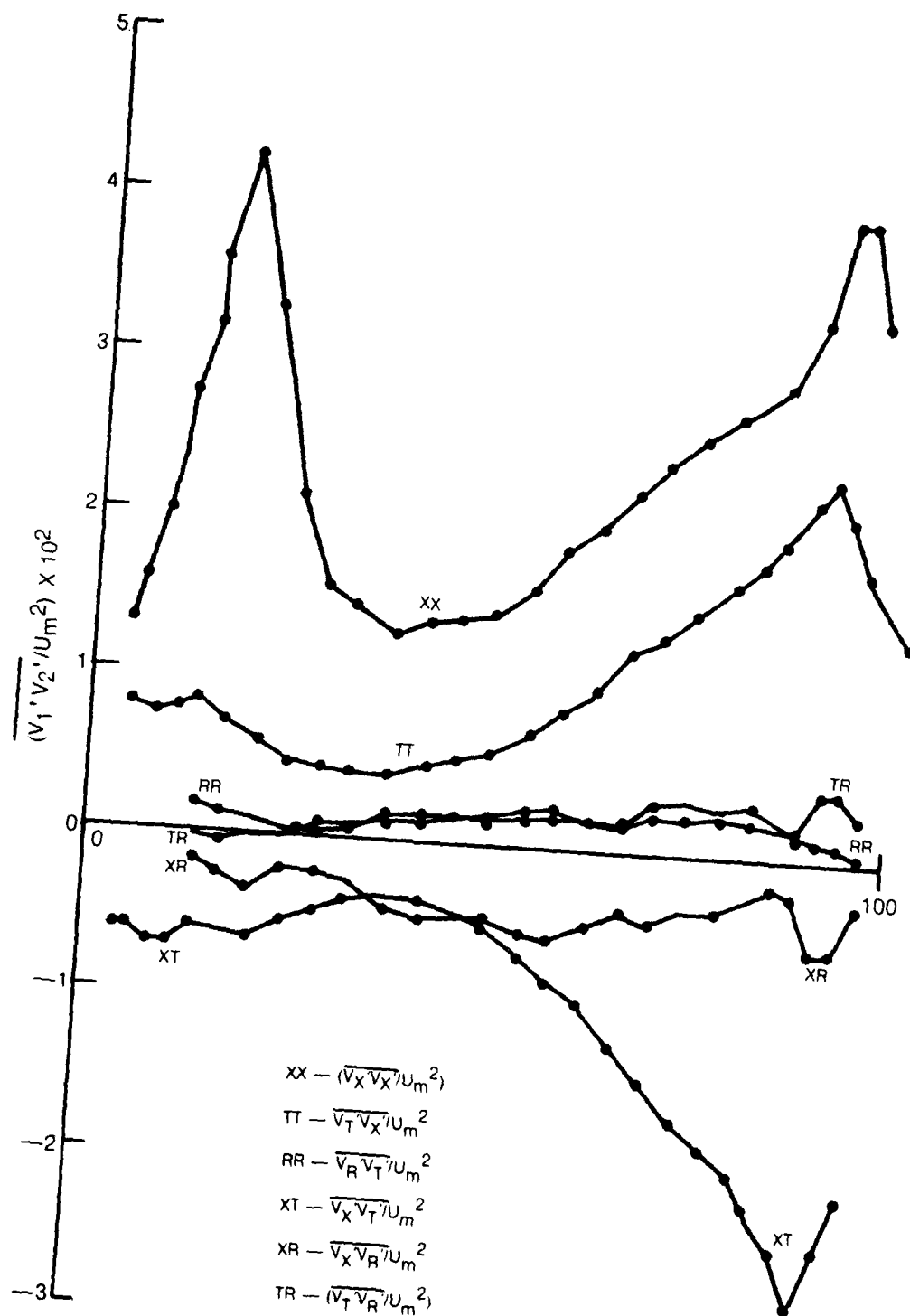Figure 23. Spanwise Distributions of Fluctuation Terms, 10% Aft, $(C_x/U_m) = 0.85$

Figure 24. Spanwise Distributions of Fluctuation Terms, 10% Aft, $(C_x/U_m) = 0.65$

40
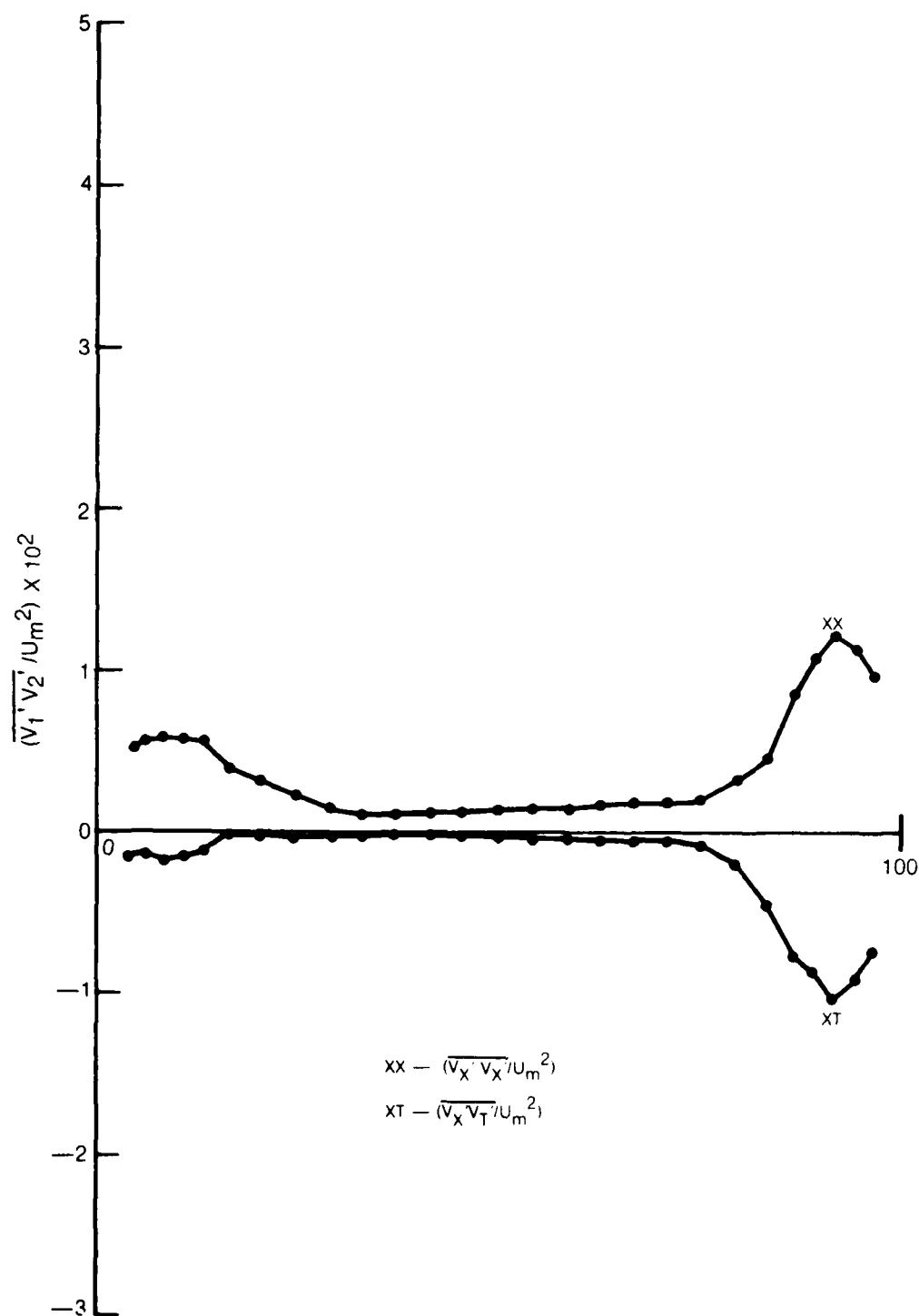
Figure 25. Spanwise Distributions of Fluctuation Terms, 50% Aft, $(C_x/U_m) = 0.65$

REFERENCES

1. Agard Conference Proceedings No. 195: Through-Flow Calculations in Axial Turbomachinery. AGARD-CP-195, October 1976.

2. Thompkins, W. T. and J. L. Kerrebrock: Exit Flow From a Transonic Compressor Rotor. Mass Inst. of Tech., Gas Turbine Lab., Report No. 123, September 1975.

3. Raj. R. and B. Lakshminarayana: Three-Dimensional Characteristics of Turbulent Wakes Behind Rotors of Axial Flow Turbomachinery. Trans. ASME, Jour. Eng. for Power, pp. 218-228, April 1976.

4. Reynolds, B., B. Lakshminarayana and A. Ravindranath: Characteristics of the Near-Wake of a Compressor or Fan Rotor Blade. AIAA Paper No. 78-1141, July 1978.

5. Ravindranath, A. and B. Lakshminarayana: Mean Velocity and Decay Characteristics of the Near- and Far-Wake of a Compressor Rotor Blade of Moderate Loading. ASME Paper No. 79-GT-202, March 1979.

6. Hirsch, C. and P. Kool: Measurement of the Three-Dimensional Flow Field Behind an Axial Compressor Stage. Trans. ASME, Jour. Eng. for Power, pp. 168-180, April 1977.

7. Kool, P., J. DeRuyck and C. Hirsch: The Three-Dimensional Flow and Blade Wake in an Axial Plane Downstream of an Axial Flow Compressor Rotor. ASME Paper No. 78-GT-66, March 1978.

8. Sehra, A. K. and J. L. Kerrebrock: The Effect of Blade-to-Blade Flow Variations on the Mean Flow-Field of a Transonic Compressor. AIAA Paper No. 79-1515, July 1979.

APPENDIX

MAGNETIC TAPE DATA FORMAT

Card type	Format
Index cards	80A1
Control card	for UTRC use
Title card	80A1
Data cards	1X, 2I4, 2F6.2, 5F8.3

        Run number
        Circ. sequence number
        Radial position (ins. from center line)
        Circumferential position (degrees from reference location)
        Total Pressure Coefficient
        Static Pressure Coefficient
        (C_x/U_m)
        Yaw (degrees)
        Pitch (degrees)

Control card	for UTRC use

    A sample of the data format is provided on the following page where the first 98 lines have been listed. Lines 1 through 18 are the Index cards describing the location of the various planes of data for each axial location and for each value of (C_x/U_m). Line 19 is a Control card. Line 20 is a Title card. Lines 21 through 58 are Data cards for the thirty-eight circumferential locations at which data was obtained at a radius of 24.25 inches, 0.25 inches from the hub. This is Cobra probe data and hence the pitch angle (listed in the right hand column) is zero. Line 59 is is a Control card. Lines 60 through 97 are the data cards for the 24.35 inch radial position. Line 98 is a Control card. This sequence continues with increasing radius down to line number 1131 (as indicated in line 2 of the index). At line 1132 the data for a different (C_x/U_m) begins.

43

```
 1:C          INDEX
 2:C     X/BX = 0.10,   CX/U = 0.650,  LINES     19 -  1131
 3:C     X/BX = 0.10,   CX/U = 0.750,  LINES   1132 -  1924
 4:C     X/BX = 0.10,   CX/U = 0.850,  LINES   1925 -  2969
 5:C     X/BX = 0.10,   CX/U = 0.950,  LINES   2970 -  3765
 6:C     X/BX = 0.30,   CX/U = 0.650,  LINES   3766 -  4635
 7:C     X/BX = 0.30,   CX/U = 0.750,  LINES   4636 -  5460
 8:C     X/BX = 0.30,   CX/U = 0.850,  LINES   5461 -  6329
 9:C     X/BX = 0.30,   CX/U = 0.950,  LINES   6330 -  7239
10:C     X/BX = 0.50,   CX/U = 0.650,  LINES   7240 -  8107
11:C     X/BX = 0.50,   CX/U = 0.750,  LINES   8108 -  8686
12:C     X/BX = 0.50,   CX/U = 0.850,  LINES   8687 -  9647
13:C     X/BX = 0.50,   CX/U = 0.950,  LINES   9648 - 10525
14:C     X/BX = 1.10,   CX/U = 0.650,  LINES  10526 - 11303
15:C     X/BX = 1.10,   CX/U = 0.750,  LINES  11304 - 12198
16:C     X/BX = 1.10,   CX/U = 0.850,  LINES  12199 - 13291
17:C     X/BX = 1.10,   CX/U = 0.950,  LINES  13292 - 14168
18:C
19:     -      1     0     0     5.0000    12.8570       .0000
20:LSRR  ISOLATED  ROTOR,  X/BX=0.10,  CX/UM  =  0.650
21:     26     1  24.25   5.00     -.634     -.036      .650  -12.919      .000
22:     26     2  24.25   6.00     -.629     -.066      .651   -7.264      .000
23:     26     3  24.25   6.99     -.607     -.086      .651   -6.992      .000
24:     26     4  24.25   8.01     -.620     -.111      .652   -9.6[illegible]      .000
25:     26     5  24.25   8.99     -.635     -.126      .652  -10.063      .000
26:     26     6  24.25  10.00     -.679     -.141      .651  -11.426      .000
27:     26     7  24.25  11.00     -.736     -.166      .651  -11.501      .000
28:     28     8  24.25  11.51     -.761     -.164      .650  -11.719      .000
29:     26     9  24.25  12.00     -.786     -.166      .649  -12.192      .000
30:     26    10  24.25  12.25     -.792     -.157      .649  -11.901      .000
31:     26    11  24.25  12.50     -.801     -.154      .650  -11.901      .000
32:     26    12  24.25  12.75     -.808     -.146      .651  -11.901      .000
33:     28    13  24.25  13.00     -.812     -.139      .651  -12.010      .000
34:     26    14  24.25  13.24     -.809     -.122      .650  -12.119      .000
35:     26    15  24.25  13.50     -.812     -.100      .651  -12.701      .000
36:     26    16  24.25  13.75     -.795     -.019      .651  -14.300      .000
37:     28    17  24.25  14.00     -.421      .082      .651  -26.607      .000
38:     28    18  24.25  14.25     -.054     -.030      .650    3.296      .000
39:     26    19  24.25  14.50     -.147     -.029      .652   27.292      .000
40:     26    20  24.25  14.75     -.214     -.020      .652   17.148      .000
41:     26    21  24.25  15.00     -.309     -.014      .650   11.404      .000
42:     26    22  24.25  15.24     -.381      .007      .651    8.095      .000
43:     28    23  24.25  15.49     -.456      .009      .651    5.187      .000
44:     26    24  24.25  15.75     -.525      .010      .649    2.278      .000
45:     28    25  24.25  16.00     -.582      .008      .651     .061      .000
46:     28    26  24.25  16.24     -.626      .000      .651   -2.339      .000
47:     26    27  24.25  16.50     -.641     -.004      .650   -3.666      .000
48:     26    28  24.25  16.75     -.648     -.013      .650   -4.464      .000
49:     26    29  24.25  17.00     -.659     -.035      .651   -5.575      .000
50:     26    30  24.25  17.50     -.669     -.040      .649   -7.574      .000
51:     28    31  24.25  17.99     -.671     -.054      .649   -8.011      .000
52:     26    32  24.25  19.01     -.655     -.088      .651   -9.683      .000
53:     26    33  24.25  20.00     -.652     -.097      .653  -10.701      .000
54:     28    34  24.25  21.00     -.634     -.130      .652  -11.101      .000
55:     28    35  24.25  22.01     -.647     -.117      .653  -10.919      .000
56:     28    36  24.25  23.00     -.681     -.144      .650  -10.610      .000
57:     26    37  24.25  24.00     -.737     -.166      .651  -11.210      .000
58:     26    38  24.25  25.01     -.783     -.156      .652  -11.392      .000
59:1
60:     28     1  24.35   5.00     -.753     -.050      .651  -14.918      .000
61:     28     2  24.35   5.99     -.750     -.080      .650  -11.210      .000
62:     26     3  24.35   7.00     -.738     -.099      .650  -12.992      .000
63:     26     4  24.35   8.01     -.731     -.123      .650  -13.573      .000
64:     28     5  24.35   8.99     -.740     -.125      .649  -14.409      .000
65:     26     6  24.35  10.01     -.759     -.150      .651  -14.337      .000
66:     28     7  24.35  11.00     -.792     -.164      .651  -14.337      .000
67:     28     8  24.35  11.51     -.741     -.156      .651  -13.937      .000
68:     28     9  24.35  12.00     -.813     -.175      .651  -13.537      .000
69:     26    10  24.35  12.25     -.821     -.166      .651  -13.355      .000
70:     28    11  24.35  12.49     -.823     -.162      .650  -13.101      .000
71:     28    12  24.35  12.75     -.823     -.152      .651  -12.919      .000
72:     26    13  24.35  13.00     -.822     -.155      .651  -12.919      .000
73:     28    14  24.35  13.25     -.827     -.143      .650  -12.919      .000
74:     26    15  24.35  13.50     -.826     -.120      .651  -13.137      .000
75:     28    16  24.35  13.75     -.824     -.073      .651  -14.010      .000
76:     28    17  24.35  14.00     -.700      .078      .649  -19.936      .000
77:     28    18  24.35  14.25     -.130     -.076      .650  -35.969      .000
78:     28    19  24.35  14.50     -.168     -.051      .650   18.639      .000
79:     28    20  24.35  14.75     -.239     -.046      .651   12.531      .000
80:     28    21  24.35  15.00     -.315     -.031      .650    7.986      .000
81:     26    22  24.35  15.24     -.375     -.023      .650    5.950      .000
82:     28    23  24.35  15.49     -.466     -.009      .650    4.060      .000
83:     28    24  24.35  15.75     -.572      .000      .650    1.442      .000
84:     28    25  24.35  15.99     -.675      .023      .650   -1.066      .000
85:     28    26  24.35  16.24     -.751      .030      .649   -4.593      .000
86:     26    27  24.35  16.50     -.773     -.029      .651   -6.484      .000
87:     28    28  24.35  16.75     -.777     -.050      .652   -7.974      .000
88:     28    29  24.35  17.00     -.775     -.046      .651   -8.701      .000
89:     26    30  24.35  17.50     -.779     -.061      .651   -9.792      .000
90:     28    31  24.35  18.00     -.776     -.072      .651  -10.810      .000
91:     26    32  24.35  19.00     -.766     -.099      .650  -12.555      .000
92:     28    33  24.35  20.00     -.751     -.111      .650  -13.537      .000
93:     28    34  24.35  21.00     -.749     -.120      .650  -14.409      .000
94:     26    35  24.35  22.01     -.744     -.131      .650  -14.664      .000
95:     28    36  24.35  22.99     -.765     -.137      .650  -14.846      .000
96:     26    37  24.35  23.99     -.793     -.166      .650  -13.937      .000
97:     26    38  24.35  24.99     -.814     -.168      .651  -12.882      .000
98:1
```

LINE NO
RUN NO
CIRC SEQUENCE NO
RADIAL POSITION
CIRCUMFERENTIAL POSITION
TOTAL PRESSURE COEFFICIENT
STATIC PRESSURE COEFFICIENT
(C_x/U_m)
YAW
PITCH

THIS PAGE IS BEST QUALITY PRACTICABLE
FROM COPY FURNISHED TO DDC

79-12-130-1

☆U.S.Government Printing Office: 1980 — 657-084/496